2007-12

Free Electron Laser performance with quadrupole magnet misalignment from shipboard vibrations

Burggraff, David T.

Monterey, California. Naval Postgraduate School

NAVAL POSTGRADUATE SCHOOL

MONTEREY, CALIFORNIA

THESIS

FREE ELECTRON LASER PERFORMANCE WITH QUADRUPOLE MAGNET MISALIGNMENT FROM SHIPBOARD VIBRATIONS

by

David Thomas Burggraff

December 2007

Thesis Advisor:	William B. Colson
Second Reader:	John W. Lewellen

Approved for public release; distribution is unlimited

THIS PAGE INTENTIONALLY LEFT BLANK

REPORT DOCUMENTATION PAGE			Form Approved OMB No. 0704-0188
Public reporting burden for this collection of information is estimated to average 1 hour per response, including the time for reviewing instruction, searching existing data sources, gathering and maintaining the data needed, and completing and reviewing the collection of information. Send comments regarding this burden estimate or any other aspect of this collection of information, including suggestions for reducing this burden, to Washington headquarters Services, Directorate for Information Operations and Reports, 1215 Jefferson Davis Highway, Suite 1204, Arlington, VA 22202-4302, and to the Office of Management and Budget, Paperwork Reduction Project (0704-0188) Washington DC 20503.			
1. AGENCY USE ONLY ***(Leave blank)***	**2. REPORT DATE** December 2007	**3. REPORT TYPE AND DATES COVERED** Master's Thesis	
4. TITLE AND SUBTITLE Free Electron Laser Performance with Quadruple Magnet Misalignment from Shipboard Vibrations			**5. FUNDING NUMBERS**
6. AUTHOR(S) Burggraff, David T.			
7. PERFORMING ORGANIZATION NAME(S) AND ADDRESS(ES) Naval Postgraduate School Monterey, CA 93943-5000			**8. PERFORMING ORGANIZATION REPORT NUMBER**
9. SPONSORING /MONITORING AGENCY NAME(S) AND ADDRESS(ES) N/A			**10. SPONSORING/MONITORING AGENCY REPORT NUMBER**
11. SUPPLEMENTARY NOTES The views expressed in this thesis are those of the author and do not reflect the official policy or position of the Department of Defense or the U.S. Government.			
12a. DISTRIBUTION / AVAILABILITY STATEMENT Approved for public release; distribution is unlimited			**12b. DISTRIBUTION CODE**

13. ABSTRACT (maximum 200 words)

The Free Electron Laser (FEL) has been discussed and studied in the United States Navy's directed energy weapon efforts. The goal of these studies is to use the FEL as a ship's primary defensive weapon against incoming threats such as missiles, aircraft and small boats.

This thesis is an analysis of the effects of shipboard vibration on the performance of an FEL. The focus of this analysis will be on the performance degradation due to quadrupole magnet misalignments from ship vibrations and flexing.

This study is aimed at improving system design efforts by determining the sensitivity of an FEL on magnet misalignments due to shipboard vibration and flexing. Simulations were conducted on the magnets placed along the electron beam path between the end of the accelerator and the beginning of the undulator. Simulations within this study were conducted using the 3D FEL simulator designed and programmed at the Navy Postgraduate School and FELSIM designed and managed by Advanced Energy Systems.

14. SUBJECT TERMS Free Electron Laser, FEL, Directed Energy, Quadrupole, Magnet Misalignment			**15. NUMBER OF PAGES** 79
			16. PRICE CODE
17. SECURITY CLASSIFICATION OF REPORT Unclassified	**18. SECURITY CLASSIFICATION OF THIS PAGE** Unclassified	**19. SECURITY CLASSIFICATION OF ABSTRACT** Unclassified	**20. LIMITATION OF ABSTRACT** UU

NSN 7540-01-280-5500

Standard Form 298 (Rev. 2-89)
Prescribed by ANSI Std. 239-18

THIS PAGE INTENTIONALLY LEFT BLANK

Approved for public release; distribution is unlimited

FREE ELECTRON LASER PERFORMANCE WITH QUADRUPOLE MAGNET MISALIGNMENT FROM SHIPBOARD VIBRATIONS

David T. Burggraff
Lieutenant, United States Navy
B.S., Texas A&M University, 2003

Submitted in partial fulfillment of the
requirements for the degree of

MASTER OF SCIENCE IN APPLIED PHYSICS

from the

NAVAL POSTGRADUATE SCHOOL
December 2007

Author: David T. Burggraff

Approved by: William B. Colson
Thesis Advisor

John W. Lewellen
Second Reader

James H. Luscombe
Chairman, Department of Physics

THIS PAGE INTENTIONALLY LEFT BLANK

ABSTRACT

The Free Electron Laser (FEL) has been discussed and studied in the United States Navy's directed energy weapon efforts. The goal of these studies is to use the FEL as a ship's primary defensive weapon against incoming threats such as missiles, aircraft and small boats.

This thesis is an analysis of the effects of shipboard vibration on the performance of an FEL. The focus of this analysis will be on the performance degradation due to quadrupole magnet misalignments from ship vibrations and flexing.

This study is aimed at improving system design efforts by determining the sensitivity of an FEL on magnet misalignments due to shipboard vibration and flexing. Simulations were conducted on the magnets placed along the electron beam path between the end of the accelerator and the beginning of the undulator. Simulations within this study were conducted using the 3D FEL simulator designed and programmed at the Navy Postgraduate School and FELSIM designed and managed by Advanced Energy Systems.

THIS PAGE INTENTIONALLY LEFT BLANK

TABLE OF CONTENTS

LIST OF FIGURES

THIS PAGE INTENTIONALLY LEFT BLANK

LIST OF TABLES

THIS PAGE INTENTIONALLY LEFT BLANK

LIST OF ACRONYMS AND ABBREVIATIONS

AES	Advanced Energy Systems
cm	Centimeters
FEL	Free Electron Laser
GUI	Graphical user interface
Hz	Hertz
K	Kelvin
LANL	Los Alamos National Laboratory
m	Meter
mm	Millimeters
mrad	Milliradian
MeV	Mega-Electron Volt
MHz	Mega-Hertz
MW	Mega-Watt
NPS	Naval Postgraduate School
rad	Radian
RF	Radio Frequency
SASE	Self Amplification of Spontaneous Emission
SLINAC	Superconducting Linear Accelerator
SRF	Superconducting Radio Frequency
T	Tesla
W	Watts

THIS PAGE INTENTIONALLY LEFT BLANK

LIST OF SYMBOLS

a	Optical field amplitude
a	Quadrupole semi-aperture
$\vec{A}$	Vector field potential
$\vec{B}$	Magnetic field
B	Magnetic field magnitude
$\vec{B}_o$	Magnetic field of optical field
$\vec{B}_M$	Magnetic field of the undulator
c	Speed of light
d	Drift length
e	Electron charge
$\vec{E}$	Electric field
E	Magnitude of electric field
$\vec{E}_o$	Electric field of optical field
f	Focal length
F_M	Magnetic field force
G	Optical field gain
j	Dimensionless current density
$\vec{J}_\perp$	Transverse current density
K	Undulator parameter
k	Optical wave number
k_o	Undulator wave number

L	Undulator length
L_Q	Length of quadrupole magnet
m	Electron mass
N	Number of periods
t	Time
z	Undulator direction
$\vec{\beta}$	Dimensionless electron velocity
$\beta_\perp$	Dimensionless transverse electron velocity magnitude
ϕ	Initial optical phase
γ	Lorentz factor
κ	Normalized linear field gradient
λ	Optical wavelength
λ_o	Undulator wavelength
ν	Electron phase velocity
ν_o	Initial electron phase velocity
ρ_e	Electron density
τ	Dimensionless time
ω	Optical frequency
ω	Vibration frequency
ω_0	Resonant frequency
ψ	Optical phase
ζ	Electron phase

I. INTRODUCTION

The Free Electron Laser (FEL) has long been discussed and studied in the United States Navy's directed energy weapon efforts. The goal of these studies is to use the FEL as a ship's defensive weapon against incoming threats such as missiles, aircraft and small boats. This weapon also has many offensive possibilities. The laser's high power availability and wavelength tunability make this an extremely desirable weapon, with a great advantage over the limited attributes of conventional lasers.

The FEL utilizes a beam of relativistic electrons co-propagating with an optical beam through a periodic magnetic field. This magnetic field causes the free electrons to oscillate and therefore transfer energy to an optical beam through coherent oscillation.

There have been many studies done on the effects of optical mirror misalignments on the FEL's operation and performance. However, little work has been done on the effects of components outside of the optical cavity. This is the first study that examines the effect of quadrupole magnet misalignments on the electron beam path and the overall performance degradation of the laser. This study is aimed at improving system design efforts by determining the sensitivity of an FEL to magnet misalignments due to possible shipboard vibrations. The next two chapters will briefly describe the FEL physics and components. Then the tolerance of an oscillator to electron beam shifts and tilts will be established and finally the quadrupole magnets will be misaligned to determine the effects and limits of these disturbances.

Simulations for this study were conducted using the 3D FEL simulation designed and programmed at the Navy Postgraduate School and FELSIM designed and managed by Advanced Energy Systems.

THIS PAGE INTENTIONALLY LEFT BLANK

II. FREE ELECTRON LASER COMPONENTS

The Jefferson Lab Free Electron Laser is an excellent example of the layout of components necessary for a FEL to operate and as a model of the proposed laser to be installed on a Naval vessel. This layout is illustrated in Figure 1.

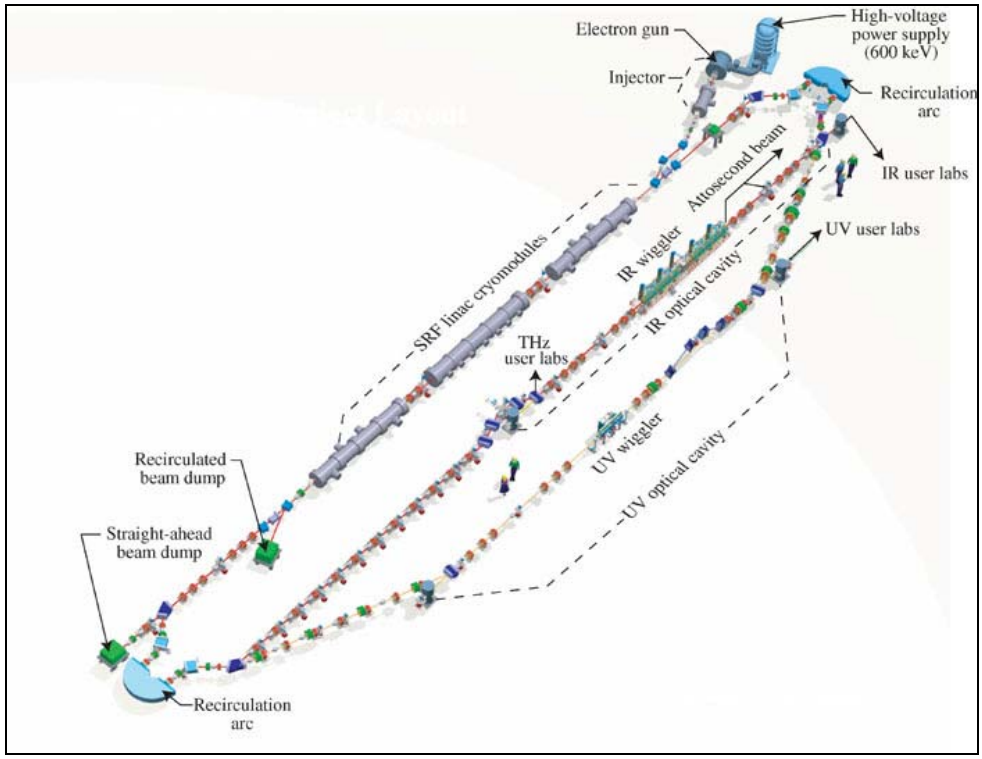

Figure 1. Jefferson Lab Free Electron Laser Layout. From [1]

The FEL operates by using a photocathode electron beam injector to send a pulsed electron beam into a superconducting linear accelerator. The electron beam's energy is increased substantially through the accelerator and directed to the wiggler (undulator) using quadrupole magnets to focus the beam and dipole magnets to deflect the path of the beam. Bending the beam path reduces the system's footprint, and is also used to condition the beam for entry into the wiggler. The electron beam enters the undulator and interacts with an optical field, leading to coherent emission as discussed in the next chapter. The electrons are then re-circulated back through the linear accelerator to recover a majority of the remaining beam energy. This increases the system's overall

efficiency, reduces the required size of the beam dump, and minimizes the need for radiation shielding. Finally the electron beam enters the beam dump.

A. AUXILIARY SYSTEMS

1. Photoinjector

The Photoinjector consists of a drive laser, photocathode and a radio frequency (RF) injector. Photoinjectors are used because of their ability to provide a high peak and average current with excellent beam quality. Photoinjectors also have the ability to be cycled on and off in picoseconds.

The drive laser is a solid-state, mode-locked laser, such as a Nd:YLF (yttrium lithium fluoride) laser, that produces an electron beam by use of a photocathode. This small, pulsed laser operates at about 700MHz. The electrons excited from the photocathode enter the synchronized RF injector that increases the electron beam energy to about 2 to 7 million electron volts (MeV). This voltage depends on the overall system design and is still being optimized.

2. Superconducting Accelerator

The superconducting linear accelerator (SLINAC) is the main energy input to the electron beam. This accelerator consists of several cavities in series that are used to increase the electron beam energy to about 100MeV using RF power. The RF is generated by a klystron and operates at the same frequency as the electron beam injector, about 700MHz. The alternating RF fields accelerate the electron bunches as they pass through each cavity. The bunches also become more compact as the slower electrons in the bunch are accelerated slightly more than the faster electrons.

These cavities are made of pure niobium due to the material's superconducting properties at temperatures below 2K. Figure 2 is a picture of a typical accelerator cavity.

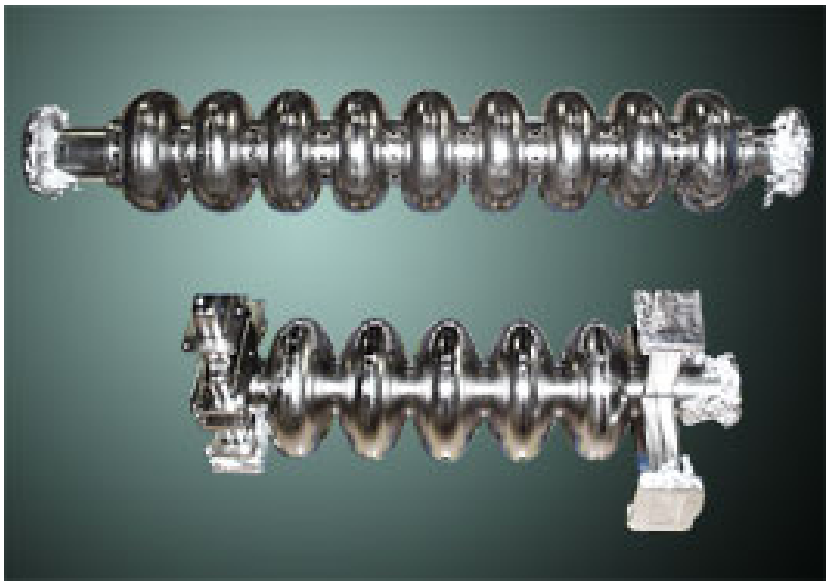

Figure 2. Superconducting Accelerator. From [1]

These cavities are cooled to below 2K using liquid helium (LHe) and a liquid nitrogen (N_2) blanket. At this temperature, the resistance in the accelerator cavity walls is on the order of nano-ohms due to impurities and defects at the material's surface.

3. Quadrupole Magnets

Quadrupole magnets are used throughout the beam path to focus and contain the beam. These magnets are placed before and after both the accelerator and undulator to focus the beam throughout the system. There are two types of quadrupole arrangements called "F" and "D". The "F" quadrupole focuses the beam in the horizontal direction while defocusing it vertically. The "D" quadrupole focuses the beam in the vertical direction while defocusing it horizontally. These two types are used conjunctively to focus the beam in both directions. They are installed in the beam path alternating between "F" and "D" types with ample separation, approximately 350mm, to prevent interference between the opposing fields. The physics of this type of magnet will be further discussed in the following chapter.

Figure 3. Quadrupole Magnet. From [2]

4. Turning Magnets

Turning, or bending, magnets are used to recirculate the electron beam back through the accelerator to reclaim its energy. They are also referred to as dipole magnets. This recirculating design also allows for a smaller system footprint. These bending magnets are designed to ensure minimal effect to the beam's energy spread. Smaller bending magnets, commonly called steering correctors, are used to fine-tune the path of the beam through the accelerator.

5. Undulator

The undulator, also called a wiggler, uses alternating dipole magnets, permanent or electromagnets, to oscillate the electron beam within its magnetic fields in the transverse direction. This motion causes the electrons to radiate light and amplify the optical beam within the optical cavity. The spacing or period, and strength of these alternating magnets affects the wavelength at which the FEL operates. A typical magnet used in an undulator has a magnetic field strength of about 1 Tesla (T). The length of the oscillator will vary based on the type of optical cavity design utilized. This will be discussed in the optical cavity section. Figure 4 is a schematic of the fields and resulting periodic motion of the electron beam in a planar undulator. A more complex undulator, known as a helical undulator, imparts a corkscrew-like helical trajectory to the beam.

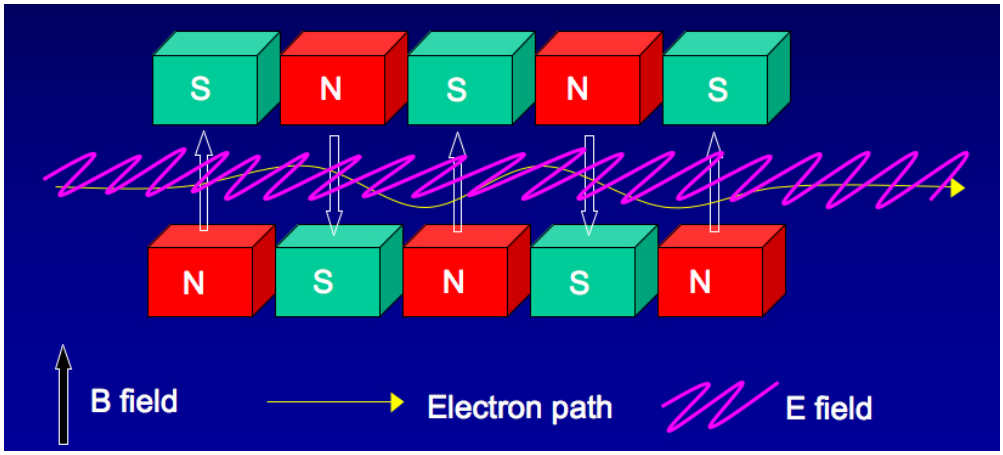

Figure 4. FEL Undulator. From [3]

6. Beam Dump

The beam dump is used to absorb the remaining energy of the electron beam once it is recirculated back through the accelerator. The electron beam reenters the accelerator roughly 180^{o} out of phase from its original transit, returning most of its energy to the accelerator and subsequently losing the remaining 5MeV of energy it still possesses by absorption in the beam dump. Beam dumps can be constructed of aluminum, copper or tungsten. This metal is externally water cooled to remove the resulting thermal energy. One large benefit of the electron beam recirculation design is the reduced beam energy being absorbed. By maintaining the discharged beam's energy below 10MeV, no fast or thermal neutrons are created, and therefore the amount of shielding required is greatly reduced.

B. OPTICAL CAVITY

There are two main types of Free Electron Lasers based on the optical cavity configuration: amplifiers and oscillators.

1. Amplifier Design

The amplifier design is a high gain, single-pass design. This configuration uses a seed laser to inject an optical beam into the undulator. The electron beam is then used to

amplify this low power optical beam, approximately 100W average power, over one pass through the undulator. The precise timing between the electron beam injection and seed laser beam is crucial for the electron pulse to overlap the optical pulse for optimal amplification. Other designs that have been recently developed do not require a seed laser. These designs are called Self Amplification of Spontaneous Emission (SASE). However, due to relatively poor optical beam quality, this design is probably not suitable for military applications. The undulator in the amplifier configuration is required to be longer than the oscillator design, about 5m in length with about 100 to 200 periods.

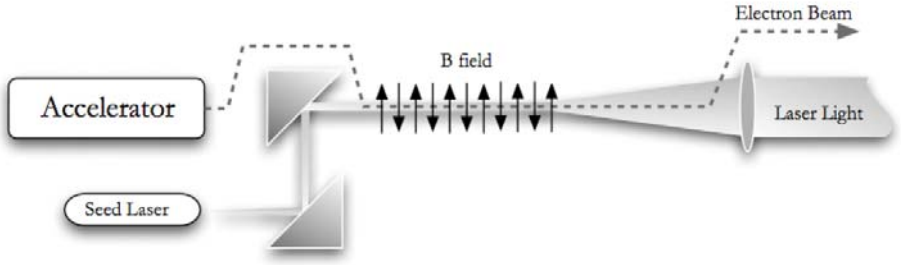

Figure 5. Amplifier Design. From [4]

2. Oscillator Design

The oscillator design uses an undulator that is placed between two mirrors, one reflective and one partially transparent (about 50% for the weapon system). This is a lower gain design that utilizes multiple optical beam passes to reach saturation. The optical beam is trapped within the optical cavity and is coupled to the electron beam in order to achieve high optical intensity through interactions with successive electron bunches.

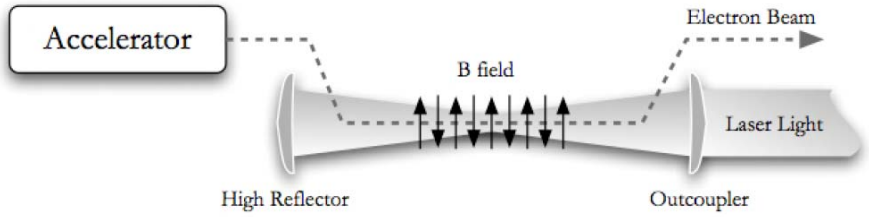

Figure 6. Oscillator Design. From [4]

The undulator can be shorter than the amplifier design, about 0.5m with about 10 to 20 periods; however the mirrors used to create the optical cavity are required to be spaced about 20m to allow for diffraction of the optical beam to reduce the intensity on the mirrors. These mirrors must also be spaced to ensure exact timing of the reflected light pulses to meet the incoming electron pulses for maximum amplification.

THIS PAGE INTENTIONALLY LEFT BLANK

III. FREE ELECTRON LASER PHYSICS

A. UNDULATOR FIELDS AND RESONANCE

The electron beam experiences three fields in the undulator: the magnetic field from the permanent magnets, the magnetic field of the optical beam and the electric field of the optical beam. The helical undulator's magnetic field due to its permanent magnets is

$$\vec{B}_M = B(\cos(k_0 z), \sin(k_0 z), 0), \tag{3.1}$$

where the undulator wave number is $k_0 = 2\pi/\lambda_0$. The undulator's period or wavelength is λ_0 and B is the magnetic field strength. The optical beam also creates magnetic and electric fields

$$\vec{B}_O = E(\sin\psi, \cos\psi, 0), \tag{3.2}$$

$$\vec{E}_O = E(\cos\psi, -\sin\psi, 0), \tag{3.3}$$

where the optical phase is $\psi = kz - \omega t + \phi$, ω is the optical frequency, ϕ is the optical phase and E is the electric field strength. The optical wave number is $k = 2\pi/\lambda$ and λ is the wavelength of the optical beam. These three fields are illustrated in Figure 7; the optical field is blue. The red line indicates the electron's path due to the magnetic field (green).

The effect that these forces have on the electron beam can be determined using the relativistic Lorentz force equations [5]

$$\frac{d(\gamma\vec{\beta})}{dt} = -\frac{e}{mc}(\vec{E} + \vec{\beta}\times\vec{B}), \tag{3.4}$$

$$\frac{d\gamma}{dt} = -\frac{e}{mc}\vec{\beta}\cdot\vec{E}, \tag{3.5}$$

$$\gamma = \left(1 - \beta^2\right)^{-1/2}, \tag{3.6}$$

where $\vec{\beta} = \vec{v}_e / c$ and $\vec{v}_e$ is the electron's velocity vector.

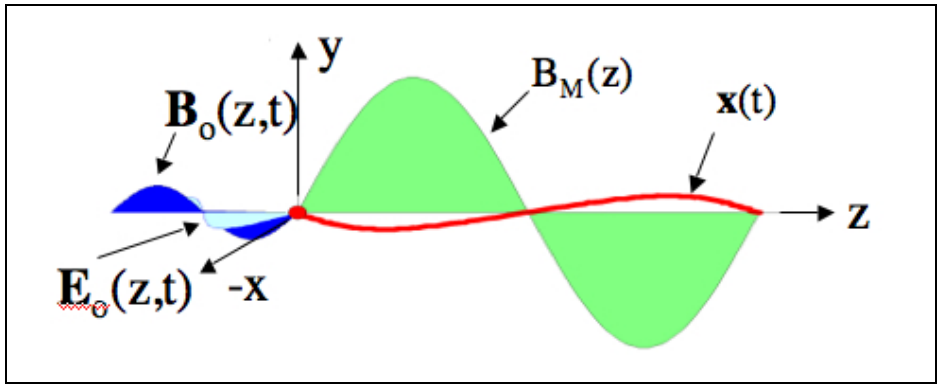

Figure 7. Undulator and Optical Fields. From [6, a]

The "resonance condition" is the required relationship between the electron beam and the optical and undulator fields for optimal energy exchange and amplification of the optical beam. This condition occurs when the optical wave travels a distance of $\lambda_0 + \lambda$ along the undulator during the time it takes the electron beam to travel one period (λ_0) along the undulator. The electrons are traveling along the z-axis slightly slower than the optical beam, which travels at the speed of light. Thus, the resonance condition allows one wavelength of light to pass the electron over a single undulator period. Figure 8 illustrates this relationship. The blue line indicates the optical wavelength and the green indicates the undulator wavelength with the red dot symbolizing the electron's position within an optical wavelength at five positions along the undulator period.

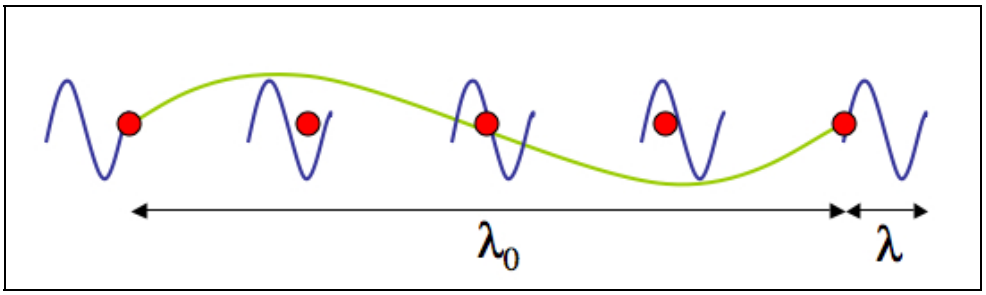

Figure 8. Electron in Resonance Condition. From [6, a]

The optical output wavelength of the FEL can be calculated using the resonance condition to obtain

$$\lambda \approx \lambda_0 \frac{(1+K^2)}{2\gamma^2}, \tag{3.7}$$

where K is the undulator parameter and is defined as $K = eB\lambda_0 / 2\pi mc^2$. Typical values of variables in equation (3.7) are $K \approx 1$ and $\gamma \approx 200$. Therefore, an undulator period λ_o of a few centimeters gives an optical wavelength of $\lambda \approx 1\mu m$. [6, b]

B. THE PENDULUM EQUATION AND ELECTRON MOTION

A combination of the three fields in the undulator determines an electron's motion. Using the Lorentz force equation (3.4) and the field equations (3.1, 3.2 and 3.3) yields the equations for transverse motion of an electron as follows:

$$\frac{d(\gamma\beta_y)}{dt} = -\frac{e}{mc}\left[-E(1-\beta_z)\sin\psi + \beta_z B\cos(k_0 z)\right], \tag{3.8}$$

$$\frac{d(\gamma\beta_x)}{dt} = -\frac{e}{mc}\left[E(1-\beta_z)\cos\psi - \beta_z B\sin(k_0 z)\right], \tag{3.9}$$

with the electrons traveling close to the speed of light, $\beta_z \approx 1$. Therefore $(1-\beta_z)$ can be neglected as it is quite small compared to the $\beta_z B$ term. Combining these two equations of motion and integrating gives the electron's transverse velocity in the undulator as

$$\vec{\beta}_\perp = -\frac{K}{\gamma}(\cos(k_0 z), \sin(k_0 z), 0), \tag{3.10}$$

where K is the undulator parameter. Using the electron/optical beam energy exchange equation described in equation (3.5) and the electron transverse velocity equation (3.10) gives the rate of change of the electron's energy as

$$\frac{d\gamma}{dt} = \frac{eKE}{\gamma mc}\cos(\zeta + \phi), \tag{3.11}$$

where the electron's phase is $\zeta = (k + k_0)z - \omega t$. Using the rate of change of the electron's energy this can also be expressed as

$$\frac{d\gamma}{dt} = \left(\frac{\gamma}{2k_0 c} \right) \frac{d^2\zeta}{dt^2}. \tag{3.12}$$

Taking the derivative of the electron phase with respect to dimensionless time $(\tau = ct/L = 0 \to 1)$ results in the electron phase velocity

$$\nu = \frac{d\zeta}{dt} = L\left[(k + k_0)\beta_z - k \right]. \tag{3.13}$$

Therefore, the change in phase velocity can be evaluated by combining the rate of change of the electron's energy equations (3.11) and (3.12) giving the equation of motion for an electron in the undulator as

$$\frac{d\nu}{dt} = \frac{d^2\zeta}{dt^2} = 2k_0 \frac{eKE}{\gamma^2 m} \cos(\zeta + \phi), \tag{3.14}$$

where $L = N\lambda_o$. Defining $|a| = 4\pi NeKLE/\gamma^2 mc^2$ as the dimensionless optical beam field amplitude, the equation of electron motion then becomes the pendulum equation

$$\frac{d\nu}{dt} = \frac{d^2\zeta}{dt^2} = |a| \cos(\zeta + \phi). \tag{3.15}$$

This equation (3.15) is used to describe the microscopic electron motion within the undulator. [6, b]

C. THE OPTICAL WAVE EQUATION

Maxwell's wave equation in the Coulomb gauge can be written as

$$\vec{\nabla}^2 \vec{A} - \frac{1}{c^2} \frac{\partial^2 \vec{A}}{\partial t^2} = -\frac{4\pi}{c} \vec{J}_\perp, \tag{3.16}$$

where $\vec{J}_\perp$ is the transverse current density and $\vec{A} = (E/k)\left[\cos\psi, -\sin\psi, 0\right]$ is the vector potential of the optical field [5]. The field amplitude and phase vary slowly over an

optical period. Using the inhomogeneous wave equation (equation (3.16)) and the slow varying amplitude and phase approximation, it is found that

$$\frac{\partial}{\partial t}(Ee^{i\phi}) = -\frac{2\pi Kec\rho_e}{\gamma}\left\langle e^{-i\zeta}\right\rangle, \qquad [3.17]$$

where ρ_e is the electron density and $\langle ... \rangle$ represents an average over all the electrons. Applying the dimensionless field amplitude, $|a(\tau)| = 4\pi NeKLE/\gamma^2 mc^2$ and dimensionless time, the wave equation can be written as follows

$$\frac{\partial a}{\partial \tau} = -j\left\langle e^{-i\zeta}\right\rangle, \qquad [3.18]$$

where $j = 8\pi^2 Ne^2K^2L^2\rho_e/\gamma^3 mc^2$ defines the dimensionless current density. [6, b]

D. GAIN AND PHASE SPACE PLOTS

1. Gain

The fractional increase of optical beam energy is defined by the optical beam gain

$$G = \frac{(|a(\tau)|^2 - a_0^2)}{a_0^2}, \qquad [3.19]$$

where a_0 is the initial optical field. At resonance the optical beam gain will be zero due to the equal energy gained and lost by the electron beam, therefore it is imperative that the electrons enter the undulator off resonance. With weak optical fields, $|a(\tau)| < \pi$, there is small bunching of the electrons and therefore a finite gain is achievable. With strong optical fields, $|a(\tau)| > \pi$, there is substantial bunching and therefore the gain becomes saturated and reduced. [6, b]

2. Phase Space Plots

Phase space plots [Figure 9] provide a profile of the motion of the electrons as they interact with the optical field over the length of the undulator.

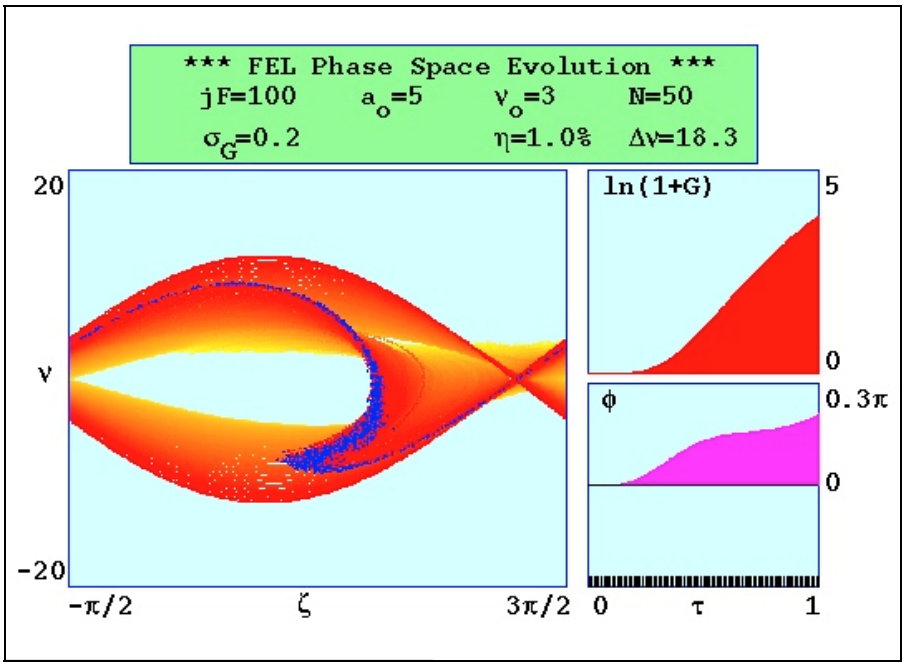

Figure 9. Sample Phase Space Plot

These plots display the relationship between the electron phase velocity (vertical axis) and the electron phase (horizontal axis) as the electrons evolve throughout the undulator. Also included in this figure are graphs of the optical gain and phase over the length of the undulator as measured in dimensionless time, τ, from 0 to 1.

This sample phase space plot was constructed using a 1-D simulation. One thousand electrons are initially equally distributed along the horizontal axis as they evolve through the undulator. In this simulation, the electrons begin at an initial phase velocity $\nu_o = 3$ in yellow, while their final position is indicated in blue. This plot indicates bunching at approximately $\zeta \approx \pi$ with a phase shift of 0.3π. The phase space plot shows a greater number of electrons losing energy to the optical beam, thus achieving high gain as shown in the upper right of Figure 9. [6, a]

IV. QUADRUPOLE MAGNET PHYSICS

In this chapter the physics that describe the effect a shift of a quadrupole magnet has on the electron beam of an FEL system will be explained. This section will use MKS units to coincide with FELSIM's input and output data.

A. DISPLACED QUADRUPOLE EQUATIONS

The magnetic field force components on an electron traveling through an "F" quadrupole (focusing in the horizontal x direction) are defined in the x and y directions as

$$F_{Mx} = -\frac{Be}{a}\left(x + \Delta x\right)\cdot v_z \quad \text{and} \tag{4.1}$$

$$F_{My} = \frac{Be}{a}\left(y + \Delta y\right)\cdot v_z, \tag{4.2}$$

where Δx and Δy are the quadrupole shift in the x and y directions respectively, $e = |e|$ is the electron charge magnitude, and v_z is the velocity of the electron in the z direction, B is the magnetic field at the pole face and a is the semi-aperture as seen on Figure 10. When the quadrupole is aligned on axis $\left(\Delta x = \Delta y = 0\right)$, an electron in the center of the quadrupole at $x = y = 0$ experiences no force. When the electron is not in the center of the quadrupole the relativistic force felt in the x and y directions result in an acceleration

$$F_x = \gamma m\frac{d^2x}{dt^2} = -\frac{eB}{a}v_z\left(x + \Delta x\right) \text{ and} \tag{4.3}$$

$$F_y = \gamma m\frac{d^2y}{dt^2} = \frac{eB}{a}v_z\left(y + \Delta y\right), \tag{4.4}$$

Where m is the electron mass, and the Lorentz Factor $\gamma = 1\Big/\sqrt{1 - v^2/c^2}$ is constant since the static magnetic field cannot change the electron's kinetic energy. Assuming $v_z \approx c$, γ is constant, v_x and $v_y \ll c$, substituting $d^2/dt^2 = c^2 \cdot d^2/dz^2$ and solving (4.3) and (4.4) for the equations of motion gives

$$\frac{d^2x}{dz^2} = -\frac{eB}{\gamma mac}\left(x + \Delta x\right) \quad \text{and} \tag{4.5}$$

$$\frac{d^2y}{dz^2} = \frac{eB}{\gamma mac}\left(y + \Delta y\right), \tag{4.6}$$

Substituting the magnetic force (4.1) into (4.5) and (4.2) into (4.6) results in the simplified equations of motion for an electron within an "F" quadrupole as

$$\frac{d^2x}{dz^2} = -\kappa\left(x + \Delta x\right) \text{ and} \tag{4.7}$$

$$\frac{d^2y}{dz^2} = \kappa\left(y + \Delta y\right), \tag{4.8}$$

where $\kappa = Be/\gamma mac > 0$ is the normalized linear field gradient. and v_z is approximately constant since γ is constant and v_x and $v_y \ll c$. Substituting $u = x + \Delta x,\ v = y + \Delta y,$ $u'' = -\kappa u$ and $v'' = \kappa v$ and solving (4.7) and (4.8) gives the position and velocity as

$$u = u_o \cos\left(\sqrt{\kappa}z\right) + \frac{1}{\sqrt{\kappa}}\left(u_o'\right)\sin\left(\sqrt{\kappa}z\right), \tag{4.9}$$

$$v = v_o \cosh\left(\sqrt{\kappa}z\right) + \frac{1}{\sqrt{\kappa}}\left(v_o'\right)\sinh\left(\sqrt{\kappa}z\right), \tag{4.10}$$

$$u' = \frac{du}{dz} = u_o\sqrt{\kappa}\sin\left(\sqrt{\kappa}z\right) + \left(u_o'\right)\cos\left(\sqrt{\kappa}z\right), \text{ and} \tag{4.11}$$

$$y' = \frac{dy}{dz} = v_o\sqrt{\kappa}\sinh\left(\sqrt{\kappa}z\right) + \left(v_o'\right)\cosh\left(\sqrt{\kappa}z\right), \tag{4.12}$$

where at $z = 0,\ u = u_o,\ v = v_o,\ u' = u_o'$, and $v' = v_o'$ are the initial positions and angles of an electron entering the quadrupole. Substituting $x_o + \Delta x = u_o,\ y_o + \Delta y = v_o,\ x_o' = u_o',$ and $y_o' = v_o'$ gives

$$x = -\Delta x + \left(x_o + \Delta x\right)\cos\left(\sqrt{\kappa}z\right) + \frac{1}{\sqrt{\kappa}}\left(x_o'\right)\sin\left(\sqrt{\kappa}z\right), \tag{4.13}$$

$$y = -\Delta y + \left(y_o + \Delta y\right)\cosh\left(\sqrt{\kappa}z\right) + \frac{1}{\sqrt{\kappa}}\left(y_o'\right)\sinh\left(\sqrt{\kappa}z\right), \tag{4.14}$$

$$x' = \frac{dx}{dz} = -\left(x_o + \Delta x\right)\sqrt{\kappa}\sin\left(\sqrt{\kappa}z\right) + \left(x_o'\right)\cos\left(\sqrt{\kappa}z\right), \text{ and} \tag{4.15}$$

$$y' = \frac{dy}{dz} = \left(y_o + \Delta y\right)\sqrt{\kappa}\sinh\left(\sqrt{\kappa}z\right) + \left(y_o'\right)\cosh\left(\sqrt{\kappa}z\right), \tag{4.16}$$

where x_o, y_o, $x_o' = dx(0)/dz$ and $y_o' = dy(0)/dz$ are the initial positions and angles of an electron entering the quadrupole.

A thin lens approximation can be used if the particle does not significantly change its transverse position within the lens. The thin-lens approximation states $\sqrt{\kappa}z << 1$. Therefore this approximation simplifies the position and velocity equations to

$$x = x_o + x_o'z, \tag{4.17}$$

$$y = y_o + y_o'z, \tag{4.18}$$

$$x' = x_o' - \left(x_o + \Delta x\right)\kappa z, \text{ and} \tag{4.19}$$

$$y' = y_o' + \left(y_o + \Delta y\right)\kappa z. \tag{4.20}$$

The focal length of the thin quadrupole lens is

$$f = \frac{1}{\kappa L_Q}, \tag{4.21}$$

where $z = L_Q$ is the length that the electrons travel through the quadrupole.

The thin lens approximation assumes that the transverse positions (x, y) of the electron does not change as it is going through the lens, only the transverse angles (x', y') changes. Taking $x_o'z$ in equation (4.17) and $y_o'z$ in equation (4.18) to be small due to the negligible change in transverse position, equations (4.17) through (4.20) become

$$x = x_o, \tag{4.22}$$

$$y = y_o, \tag{4.23}$$

$$x' = x'_o - \left(x_o + \Delta x\right)\kappa z \text{ , and} \tag{4.24}$$

$$y' = y'_o + \left(y_o + \Delta y\right)\kappa z . \tag{4.25}$$

To simplify beam transport calculations these equations are placed in matrix formalization as

$$\begin{pmatrix} x \\ x' \end{pmatrix} = \begin{pmatrix} 1 & 0 \\ -\dfrac{1}{f} & 1 \end{pmatrix}\left[\begin{pmatrix} x_o \\ x'_o \end{pmatrix} + \begin{pmatrix} \Delta x \\ 0 \end{pmatrix}\right] \text{ and} \tag{4.26}$$

$$\begin{pmatrix} y \\ y' \end{pmatrix} = \begin{pmatrix} 1 & 0 \\ \dfrac{1}{f} & 1 \end{pmatrix}\left[\begin{pmatrix} y_o \\ y'_o \end{pmatrix} + \begin{pmatrix} \Delta y \\ 0 \end{pmatrix}\right], \tag{4.27}$$

where the matrix operator changes the electron's angle $\left(x', y'\right)$ in proportion to the electron's position $\left(x_o, y_o\right)$ entering the quadrupole. This derivation has ignored the fringe field's effects, using a square edge approximation. This, however, is a good approximation for this application. With a magnetic field gradient of $B/a = 6\,\mathrm{T/m}$, the focus strength is accurate to within 10% of the full thick lens result. [7]

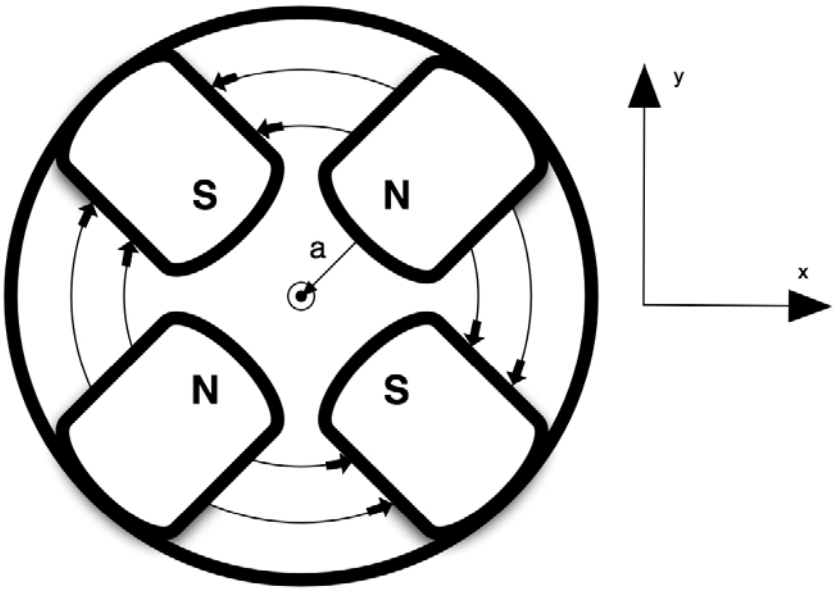

Figure 10. Quadrupole Magnet Schematic (F Type) with Electron Velocity Towards Viewer

B. DRIFT EQUATIONS

The drift space between each magnet or between a magnet and another FEL system component can be defined using the same method as with the quadrupole equations. The position and velocity equations of an electron traveling through a drift space are

$$x = x_o + x'_o z\,, \tag{4.28}$$

$$y = y_o + y'_o z\,, \tag{4.29}$$

$$x' = x'_o\,, \text{ and} \tag{4.30}$$

$$y' = y'_o\,. \tag{4.31}$$

By setting $z = d$, where d is the length an electron travels on the z axis through the drift space gives the applicable position and velocity

$$x = x_o + x'_o d\,, \tag{4.32}$$

$$y = y_o + y'_o d\,, \tag{4.33}$$

$$x' = x'_o \text{, and} \tag{4.34}$$

$$y' = y'_o \text{.} \tag{4.35}$$

Placing these equations in matrix formalization results in

$$\begin{pmatrix} x \\ x' \end{pmatrix} = \begin{pmatrix} 1 & d \\ 0 & 1 \end{pmatrix} \begin{pmatrix} x_o \\ x'_o \end{pmatrix} \text{ and} \tag{4.36}$$

$$\begin{pmatrix} y \\ y' \end{pmatrix} = \begin{pmatrix} 1 & d \\ 0 & 1 \end{pmatrix} \begin{pmatrix} y_o \\ y'_o \end{pmatrix} \text{.} \tag{4.37}$$

C. MAGNET MISALIGNMENT CALCULATION

Using the matrix formalization to calculate the effect of a quadrupole shift, it is first necessary to calculate the focal length f . Using equation (4.21), the focal length can be calculated by using the quadrupole and electron beam parameters.

Given $\kappa = Be/\gamma mav_z$, with $\gamma = 200$, $v_z = 3\times10^8\ m/s \approx c$, magnetic field gradient $B/a = 6\,\mathrm{T/m}$ for all quadrupoles used in this sample calculation, and $L_Q = 150\mathrm{mm}$ gives

$$f = \frac{1}{\kappa L_Q} = \frac{1}{\left(\frac{6.0\frac{\mathrm{T}}{\mathrm{m}} \cdot 1.6\times10^{-19}\mathrm{C}}{200 \cdot 9.1\times10^{-31}\mathrm{kg} \cdot 3\times10^8 \frac{\mathrm{m}}{\mathrm{s}}} \right) \cdot 0.15\mathrm{m}} = 0.36\mathrm{m} \tag{4.38}$$

as the focal length of the quadrupole. This gives a matrix operator for an F type quadrupole as

$$\begin{pmatrix} 1 & 0 \\ -\frac{1}{f} & 1 \end{pmatrix} = \begin{pmatrix} 1 & 0 \\ -2.75\mathrm{m}^{-1} & 1 \end{pmatrix} \text{.} \tag{4.39}$$

Each drift between the quadrupoles will be set at $d = 350\mathrm{mm}$. The matrix operator for this drift will be

$$\begin{pmatrix} 1 & d \\ 0 & 1 \end{pmatrix} = \begin{pmatrix} 1 & 0.35\text{m} \\ 0 & 1 \end{pmatrix}. \tag{4.40}$$

To calculate the resulting electron beam's transverse and angular displacement, matrix multiplication is used to find a resultant transport matrix between the quadrupole in question and the final position in z, or in this case, the start of the undulator. For purposes of a sample calculation take a set up such as: drift – quadrupole (D type) – drift – quadrupole (F type) – undulator. This transport matrix would then be

$$\underset{\text{F type}}{\begin{pmatrix} 1 & 0 \\ -2.75\text{m}^{-1} & 1 \end{pmatrix}} \underset{\text{drift}}{\begin{pmatrix} 1 & 0.35\text{m} \\ 0 & 1 \end{pmatrix}} \underset{\text{D type}}{\begin{pmatrix} 1 & 0 \\ 2.75\text{m}^{-1} & 1 \end{pmatrix}} \underset{\text{drift}}{\begin{pmatrix} 1 & 0.35\text{m} \\ 0 & 1 \end{pmatrix}} = \begin{pmatrix} -0.89 & 1.04\text{m} \\ -2.65\text{m}^{-1} & 1.96 \end{pmatrix} \tag{4.41}$$

This gives the matrix elements of the entire section as a whole. Assume that directly before this section of the beam path an F type quadrupole was shifted 1mm in the horizontal direction. The impact of the quadrupole's displacement is calculated by translating the magnet's origin so that the electron beam is offset calculating the effect on the beam in that frame and then translating back to the original reference frame. This gives

$$\begin{pmatrix} x \\ x' \end{pmatrix} = \begin{pmatrix} 1 & 0\text{m} \\ -2.75\text{m}^{-1} & 1 \end{pmatrix} \begin{pmatrix} 0.001\text{m} \\ 0 \end{pmatrix} - \begin{pmatrix} 0.001\text{m} \\ 0 \end{pmatrix} = \begin{pmatrix} 0.0\text{m} \\ -0.0028\text{rads} \end{pmatrix}; \tag{4.42}$$

note that the initial shift of a quadrupole only changes the angle of the electron beam. It is not until the electron beam travels through a following drift that there is a change in transverse position.

To calculate the final position, multiply the transport matrix (4.41) by the resulting change in beam trajectory from the 1mm quadrupole shift (4.42) to obtain

$$\begin{pmatrix} x \\ x' \end{pmatrix} = \begin{pmatrix} -0.89 & 1.04\text{m}^{-1} \\ -2.65\text{m} & 1.96 \end{pmatrix} \begin{pmatrix} 0.0\text{m} \\ -0.0028\text{rads} \end{pmatrix} = \begin{pmatrix} 0.0029\text{m} \\ -0.0055\text{rads} \end{pmatrix}. \tag{4.43}$$

Therefore, the resulting shift and tilt of the electron beam prior to entering the undulator is 2.9mm and -5.5mrads.

Due to the large number of quadrupoles used in the beam line of an FEL and the extensive calculations required to calculate the individual transport matrices for each quadrupole, a simulator (FELSIM) will be used to calculate the effects of quadrupole magnet misalignments on the electron beam's trajectory. [8]

V. FEL OSCILLATOR SIMULATIONS

A. 3D FEL OSCILLATOR MODELING PARAMETERS

It is necessary to first understand the tolerance of a 1MW FEL to an electron beam shift and/or tilt before analyzing the effects of quadrupole magnet displacements on the FEL's performance. These tolerances will be examined using the NPS Apple Xserve cluster with 128 processors. The 3D FEL Oscillator Simulator will be used to record the FEL's response to electron beam shifts and tilts and the corresponding gain and extraction for each shift will be recorded.

The properties of the electron beam entering the undulator are listed in Table 1. These values are the same values that will be used in all future simulations including FELSIM runs for the quadrupole magnet manipulations. 2.1×10^{14}

ELECTRON BEAM PARAMETERS		
Eb	Beam energy (MeV)	97.8
qbunch	Bunch charge (nC)	0.613
rbx	Beam radius, x rms (mm)	0.10
rby	Beam radius, y rms (mm)	0.10
tb	Pulse duration, FWHM (ps)	1.0
prf	Pulse rep frequency (MHz)	748.5
lb	Pulse length, FWHM (cm)	0.030
gamma	Lorentz factor	192
Ipeak	Peak current (A)	613
Iavg	Average current (mA)	459
emitx	Normalized rms x emittance (mm mrad)	2.6
emity	Normalized rms y emittance (mm mrad)	2.2
emitl	Longitudinal emittance (keV ps)	34
dgog	Beam energy spread (%)	0.08
dthetax	Beam angular spread, x rms (mrad)	0.14
dthetay	Beam angular spread, y rms (mrad)	0.11
rho	Beam density (1/cm^3)	2.1×10^{14}
Pb	Beam average power (MW)	45

Table 1. 1MW Electron Beam Parameters

The beam energy used is 97.8MeV. This is the energy of the electron beam exiting the SLINAC and traveling through the quadrupoles to the undulator. The electron pulses will be 0.03cm long with a repetition of 748.5MHz.

Table 2 gives the parameters for the undulator. The undulator length, 59cm, is typical for an oscillator configuration. The length of the undulator period is 2.95cm with a total number of periods (N) of 20.

UNDULATOR PARAMETERS		
lambda0	Undulator period (cm)	2.95
N	Number of periods	20
gap	Undulator gap (cm)	1
Bpeak	Undulator peak magnetic field (T)	0.88
Brms	Undulator magnetic field, rms (T)	0.62
K	Undulator parameter, rms	1.72
L	Undulator length (cm)	59

Table 2. 1MW Oscillator Undulator Parameters

The optical cavity parameters are listed in Table 3. With the oscillator design, a long cavity length of 20m is required. This is the distance from the reflective mirror to the semi-transparent mirror within the cavity. The optical wavelength is 1.6 μm, a desired wavelength for minimal atmospheric attenuation of a megawatt-class laser. The semi-transparent mirror has a quality factor of 2.0, corresponding to a transmission of 50% of the optical energy in the cavity on each pass.

OPTICAL CAVITY PARAMETERS		
S	Cavity length (m)	20
Z0	Rayleigh length (cm)	6
loss	Mirror losses per pass (%)	50
lambda	Optical wavelength (microns)	1.6
W0	Mode waist radius, 1/e (mm)	0.17
Wmir	Mode radius at mirrors, 1/e (cm)	2.9
Qn	Quality factor	2.0
eta	Predicted extraction (%)	2.5
Pout	Predicted output power (MW)	1.1
Imir	Optical intensity at mirrors (kW/cm^2)	86

Table 3. 1MW Oscillator Optical Cavity Parameters

Dimensionless parameters are required for the FEL simulations. These parameters are the direct inputs into the simulation and are calculated using the design parameters in Tables 1, 2 and 3. These dimensionless parameters are listed in Table 4.

DIMENSIONLESS PARAMETERS		
jhel	Normalized current density, helical undulator	135
jlin	Normalized current density, linear undulator	83
jlinF	Current density with filling factor	11.7
Gwf,lg	Predicted weak-field low gain (%)	158
Ghg	Predicted high gain (%)	252
sx	Normalized beam radius	0.18
sy	Normalized beam radius	0.18
stx	Normalized beam angular spread	0.15
sty	Normalized beam angular spread	0.12
sve	Phase velocity spread due to emittance	0.09
svg	Phase velocity spread due to energy spread	0.21
sigz	Normalized pulse length	9.5
z0	Normalized Rayleigh length	0.10
w0	Normalized mode waist radius	0.32
wmir	Normalized mode radius at mirrors	53
F	Filling factor	0.14
tmir	Normalized mirror separation	34
wbeta	Betatron oscillation frequency	1.1
xi	Bessel function argument	0.37
JJ	Bessel function factor	0.78

Table 4. Dimensionless Parameters

B. ELECTRON BEAM SHIFT IN THE VERTICAL (y) DIRECTION

The gain and extraction of this 1MW FEL was recorded for different values of electron beam shift in the vertical direction. Simulations were conducted to discover the FEL's tolerance of magnet shifts. It is only necessary to measure this parameter in one direction (positive) due to the symmetry of the undulator.

1. Gain

Figure 11 is a graph of gain versus vertical electron beam shift. This graph indicates a maximum gain of 186% with the electron beam aligned on its reference trajectory (undulator axis). However, with a shift of the electron beam in the vertical direction, the gain is dramatically reduced. In order for the FEL to sustain operations, the gain must remain above 100%. At about 1.5mm of beam shift, the gain drops below 100% indicating the FEL no longer is functional.

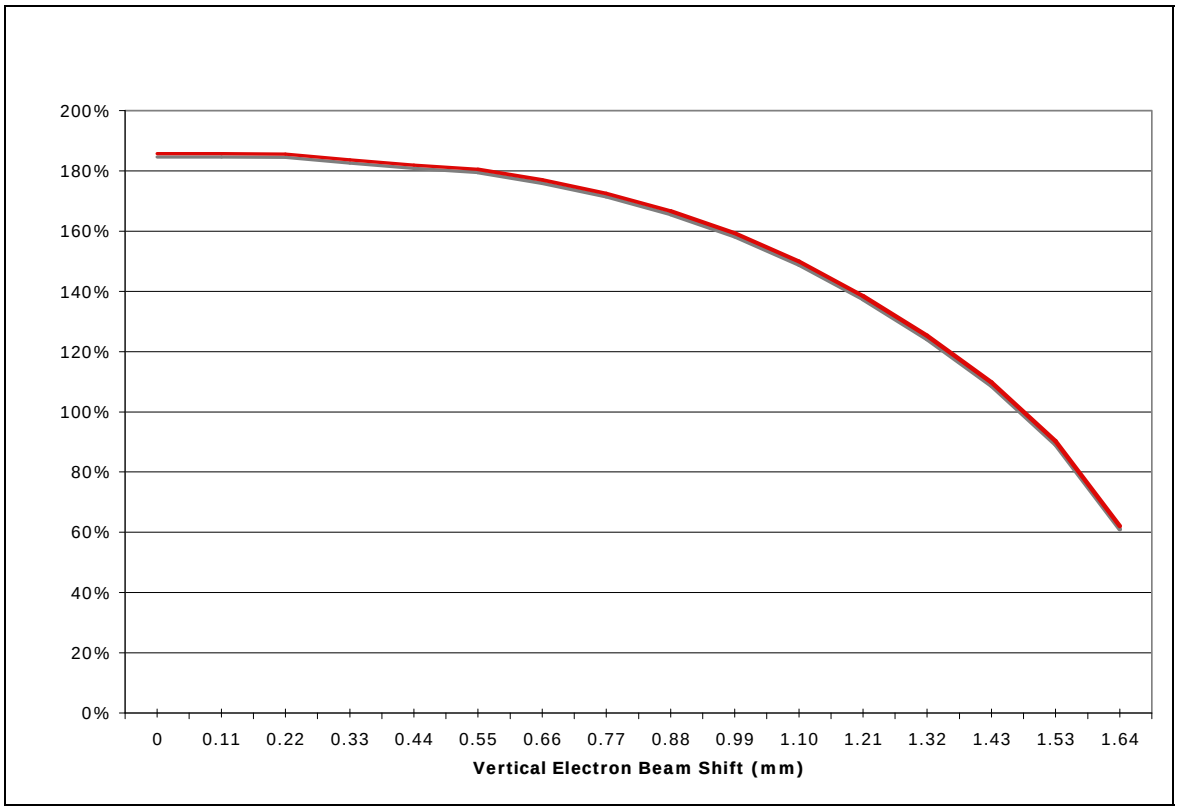

Figure 11. Gain vs. Vertical Electron Beam Shift

2. Extraction

Another useful indicator of FEL performance is the system's extraction. Figure 12 is a plot of extraction as a function of vertical electron beam shift. With no shift of the electron beam the extraction is 2.78%. With a beam average power of 45MW, as indicated on Table 1, this extraction will produce an optical power of 1.25MW.

Achieving a 1MW laser weapon requires an extraction of at least 2.2%. At about a vertical shift of 0.6mm, the extraction decreases to 2.2%. It can also be seen that there is no extraction at approximately 1.5mm of vertical shift indicating that the FEL is no longer functional. This is as predicted from the previous gain plot that indicated failure at 1.5% when gain fell to less than 100%.

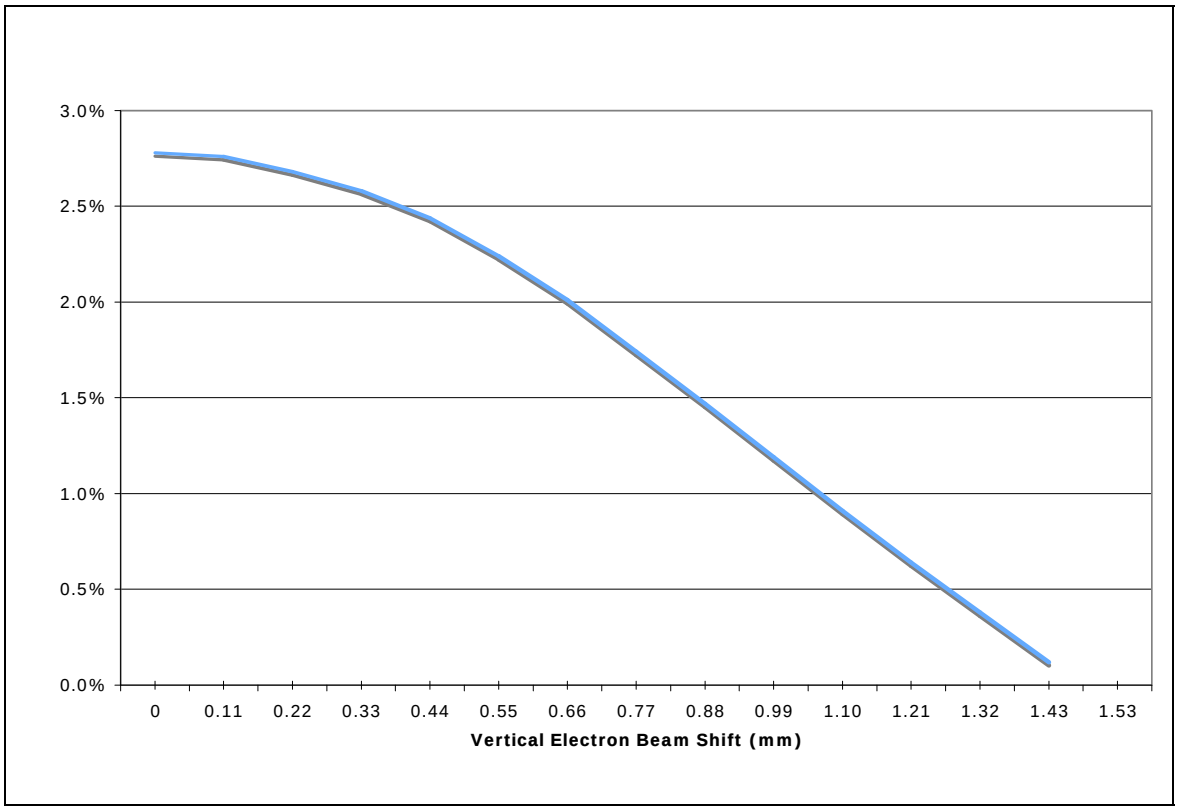

Figure 12. Extraction vs. Vertical Electron Beam Shift

The simulations of both gain and extraction for this 1MW oscillator configuration indicate that the FEL will cease to function with an electron beam shift in the vertical (y) direction of 1.5mm. However to maintain a megawatt laser the extraction must remain above 2.2%. Therefore a quadrupole magnet displacement resulting in a 0.6mm electron beam displacement in the vertical (y) direction will be the maximum allowable magnet shift.

C. ELECTRON BEAM SHIFT IN THE HORIZONTAL (x) DIRECTION

The gain and extraction were also analyzed for shifts in the horizontal direction. It is also only necessary to consider horizontal shifts in one direction (positive) due to the symmetry of the undulator.

1. Gain

Figure 13 is a graph of gain versus horizontal electron beam shift. This graph shows that a horizontal shift of the electron beam has a very similar effect on the gain of the system. Again, at about 1.5mm of horizontal beam shift, the gain drops below 100% indicating the FEL is no longer functional.

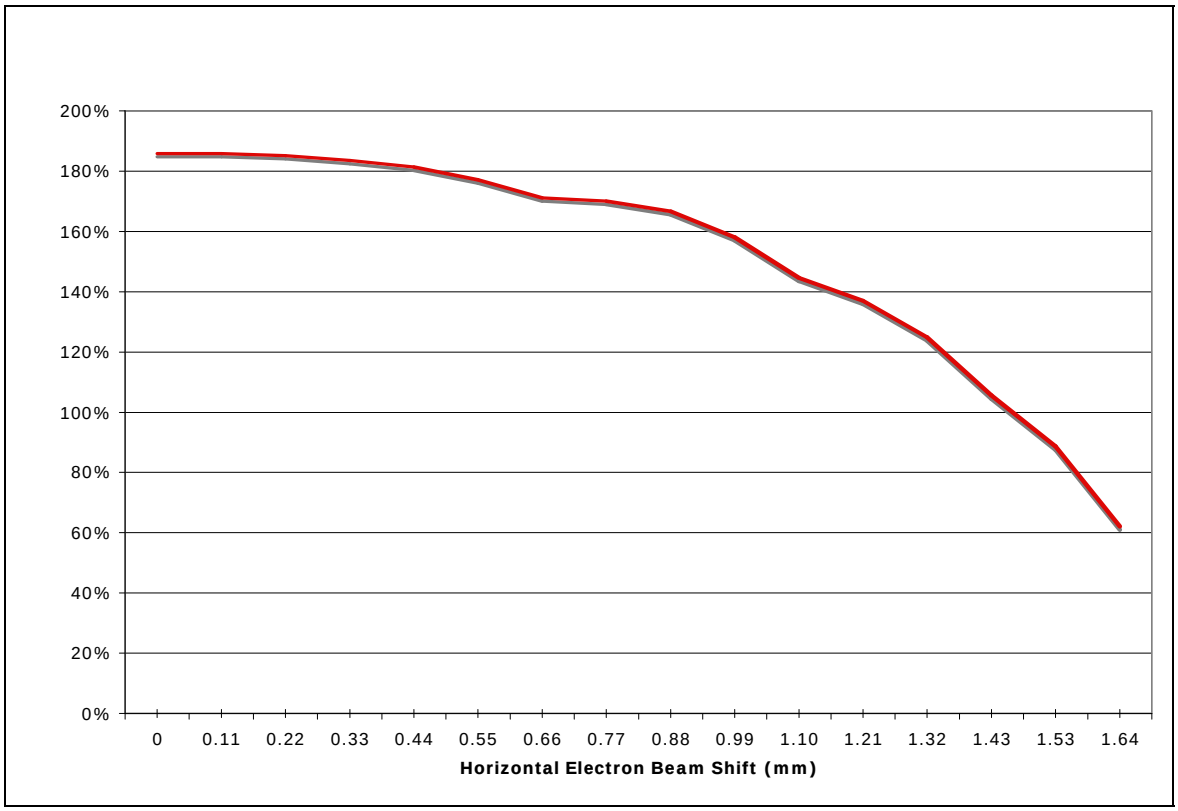

Figure 13. Gain vs. Horizontal Electron Beam Shift

This similar reaction in the horizontal shift as the vertical shift is due to the slightly concaved pole faces of the undulator magnets. This small curvature is designed to create a similar focusing effect of the electron beam in the horizontal and vertical planes.

2. Extraction

Figure 14 is a plot of extraction as a function of horizontal electron beam shift. At a horizontal beam shift of approximately 0.6mm, the extraction decreases to 2.2%.

Again, both the gain and extraction curve show agreement in FEL failure at approximately 1.5mm.

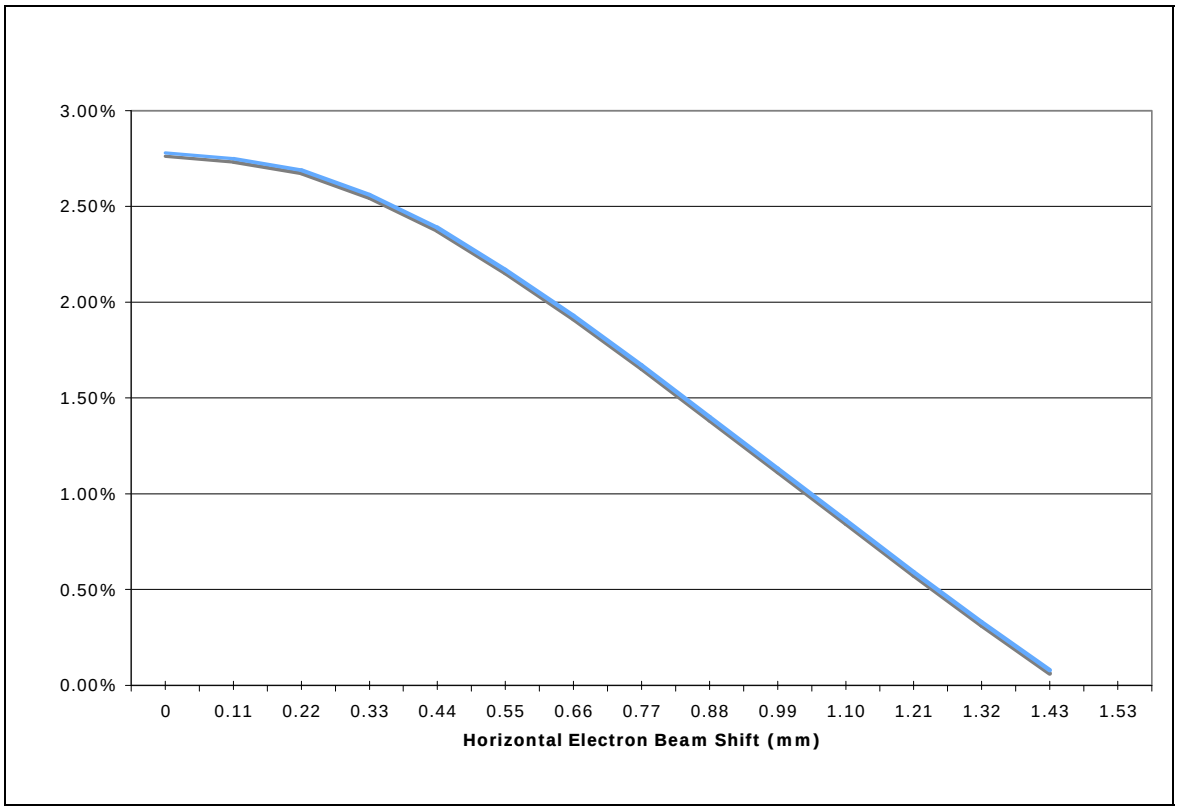

Figure 14. Extraction vs. Horizontal Electron Beam Shift

Both these results of gain and extraction were extremely close to the previous results due to a vertical electron beam shift. These results indicate the electron beam shift must remain less than 0.6mm in both directions to ensure the extraction remains above 2.2% to maintain 1MW or greater of power.

D. ELECTRON BEAM TILT IN THE VERTICAL (y) DIRECTION

As shown in Section IV, a displaced magnet will result in both a shift and tilt of the electron beam. Therefore, it is also important to analyze the FEL's tolerance to an electron beam tilt. The goals of greater than 100% gain for operation and 2.2% extraction to maintain power above 1MW still apply. It is only necessary to measure the tilt in one direction (positive) due to the symmetry of the undulator.

1. Gain

Figure 15 is a graph of gain versus vertical electron beam tilt. This graph indicates a maximum gain of 217% at an electron beam tilt of 4.65mrad. After 4.65mrad the gain reduces rapidly. An electron beam tilt in the vertical direction of about 8.1mrads will drop the gain below 100% indicating the FEL no longer is functional.

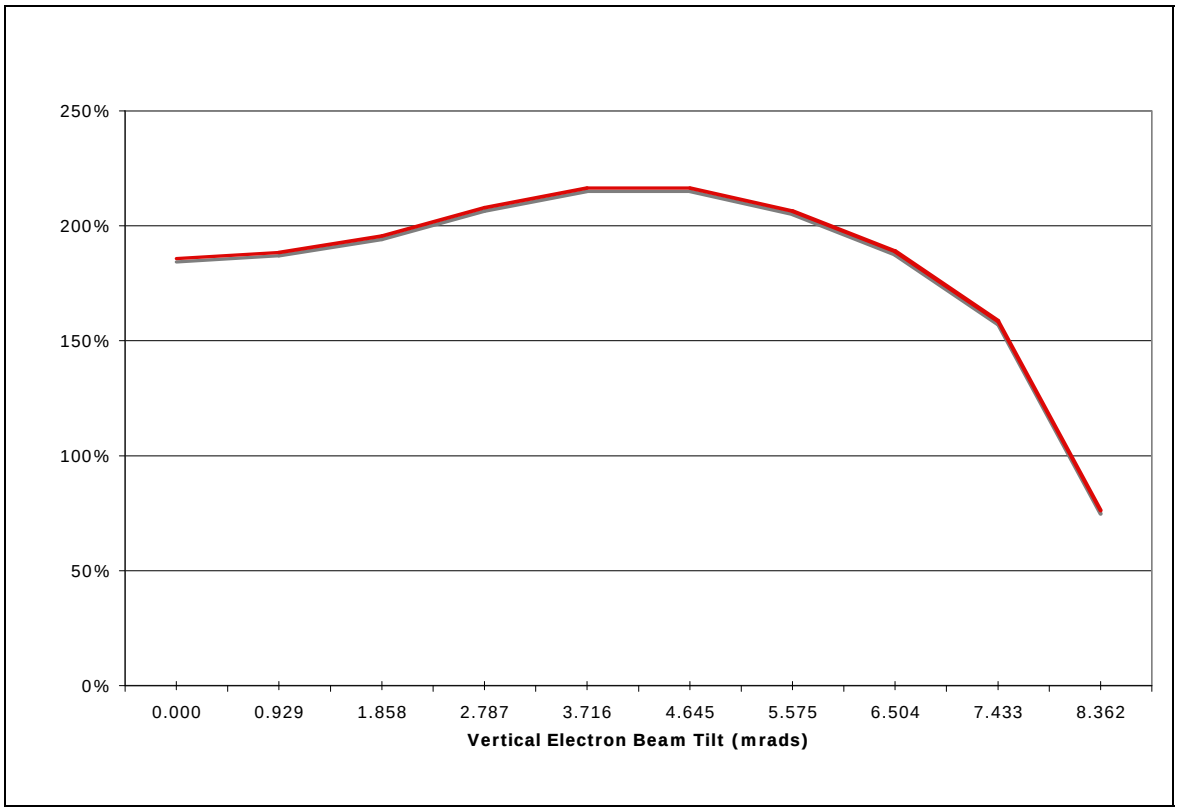

Figure 15. Gain vs. Vertical Electron Beam Tilt

2. Extraction

The extraction versus vertical electron beam tilt is shown in Figure 16. At a vertical beam tilt of 6.5mrad, the extraction decreases to 2.2%. The gain graph (Figure 15) and the extraction graph (Figure 16) show agreement in FEL failure at approximately 8.1mrads.

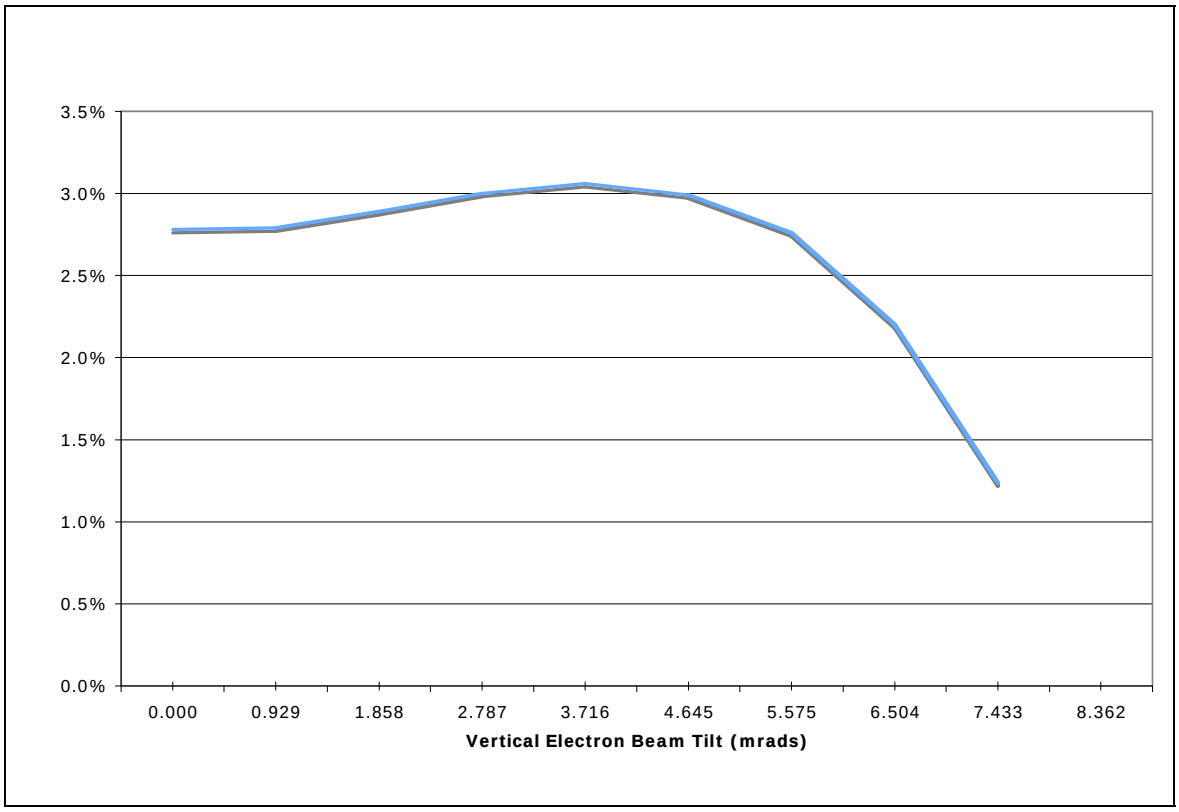

Figure 16. Extraction vs. Vertical Electron Beam Tilt

E. ELECTRON BEAM TILT IN THE HORIZONTAL (x) DIRECTION

Finally, the gain and extraction was also studied for electron beam tilts in the horizontal direction. It is only necessary to measure this parameter in one direction (positive) due to the symmetry of the undulator.

1. Gain

Figure 17 is a graph of gain versus horizontal electron beam tilt. This graph indicates that a horizontal tilt of the electron beam has an effect on the gain of the system very similar to that of the vertical tilt. Similarly, at about 8.1mrads of horizontal beam tilt results in the gain dropping below 100% indicating the FEL no longer is functional.

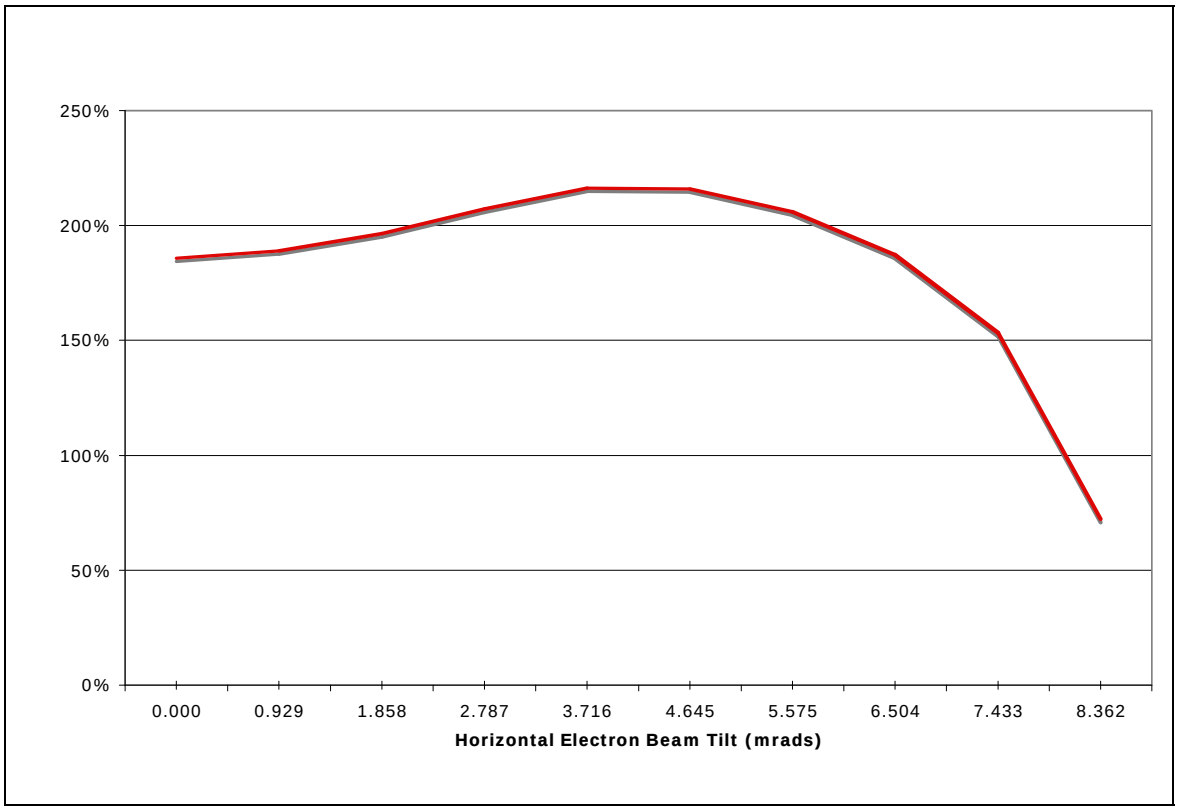

Figure 17. Gain vs. Horizontal Electron Beam Tilt

2. Extraction

Figure 18 is a plot of extraction as a function of horizontal electron beam tilt. At a horizontal beam tilt of approximately 6.5mrads, the extraction decreases to 2.2%. Again, both the gain and extraction curve show agreement in FEL failure at approximately 8.1mrads.

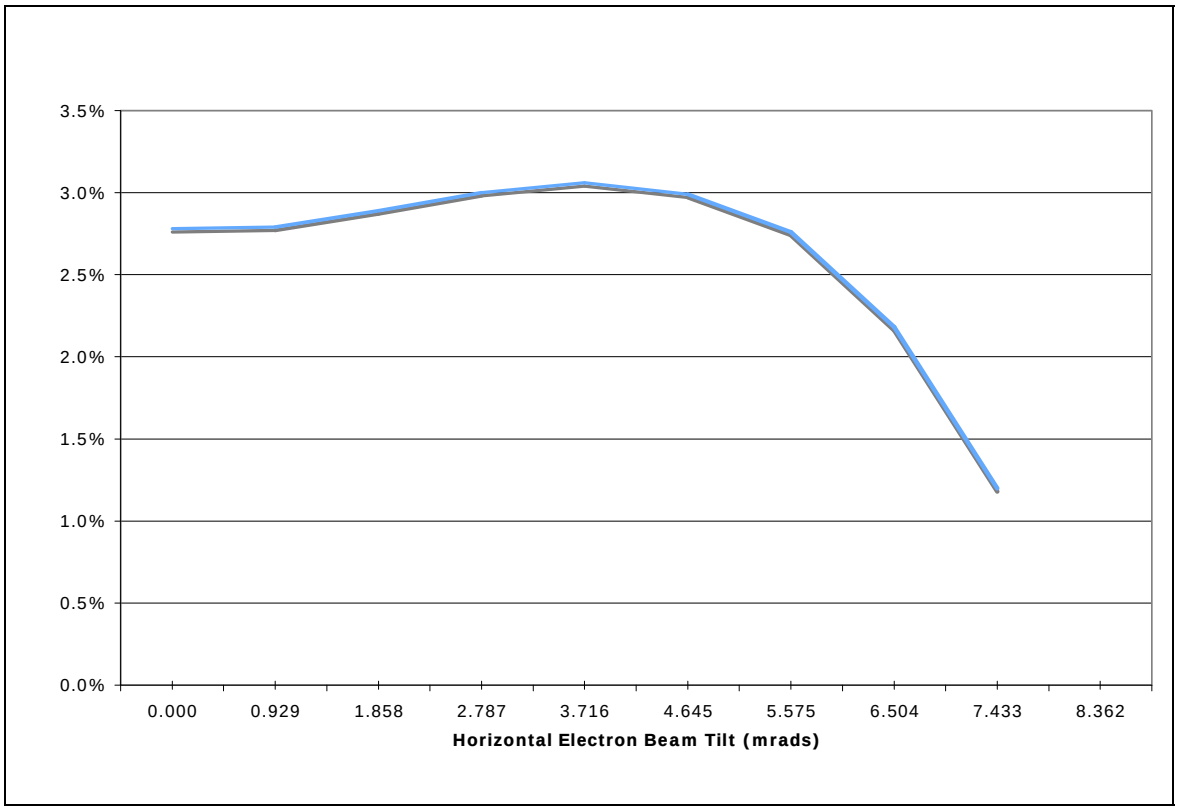

Figure 18. Extraction vs. Horizontal Electron Beam Tilt

Both the results of gain and extraction for horizontal beam tilt are extremely close to the previous results with regard to a vertical electron beam tilt. These results indicate the electron beam tilt must remain less than 6.5mrads in both the horizontal and vertical direction to ensure the extraction remains above 2.2% and therefore achieve 1MW or greater of laser power.

F. EFFECT OF ELECTON BEAM SHIFT WITH TILT COMBINATION

It has been shown that a quadrupole magnet shift will create both a shift and tilt of the electron beam when it is off reference trajectory. Therefore the effect of the combination of both displacements (both angular and transverse) must be accounted for in FEL performance.

It has also been shown in this section that the effects in the horizontal and vertical planes are extremely similar. Therefore, the following simulations and graphs have only been done in the vertical direction with the knowledge that the horizontal case would produce very similar results.

Figure 19 is a three-dimensional representation of the resultant extraction due to a shifted electron beam with a tilt entering the undulator. The vertical axis is the resultant extraction in 0.2% increments. The horizontal axis is the electron beam shift in millimeters and the final axis is the electron beam shift in milliradians. Aside from the small increase in gain at small tilt angles, the graph depicts a smooth decrease in extraction with an increase in beam shift and tilt combination, as expected.

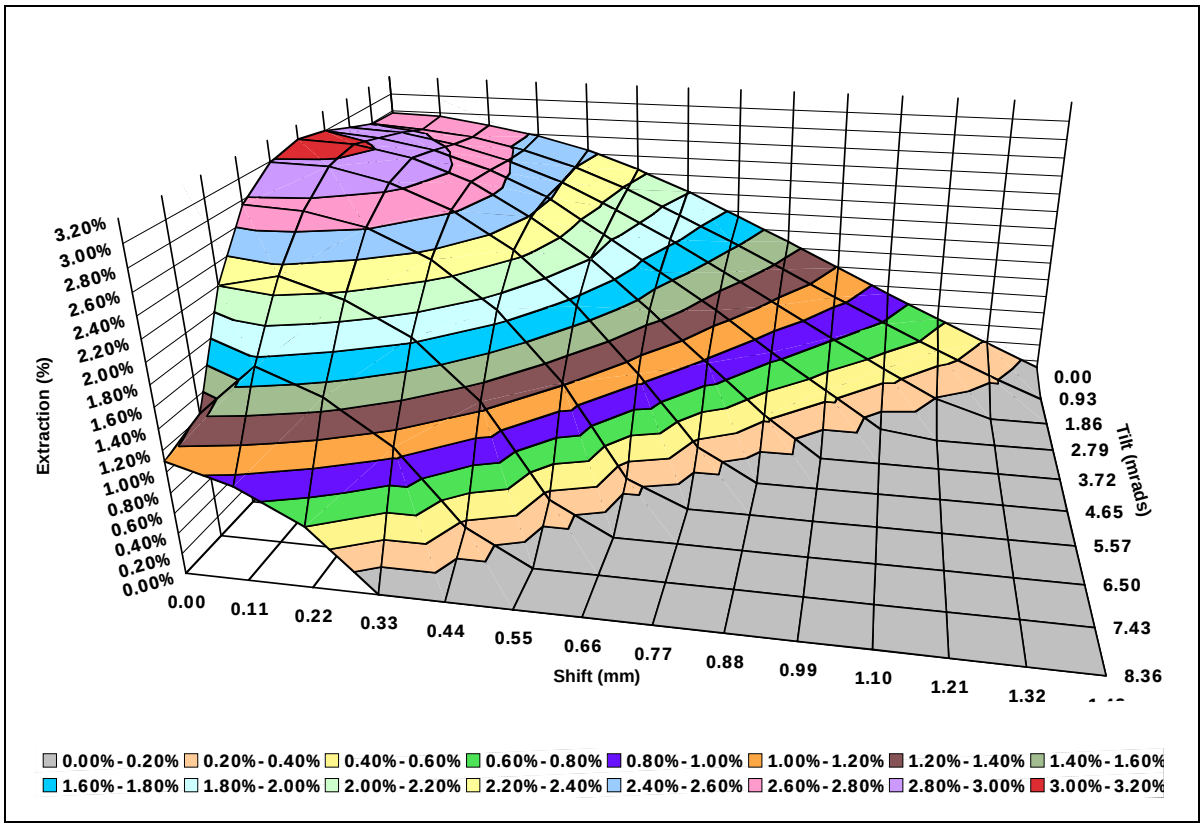

Figure 19. Extraction due to Electron Beam Shift with Tilt (3D View)

It is an interesting result that the highest extraction is not found with the beam on axis, but at no shift with a slight tilt. This is not an effect that will be explored as an optimized result because the increase in gain is so small.

With the ultimate objective of determining the maximum combined shift and tilt allowable while continuing to maintain 1MW of average power, Figure 20 clearly indicates the acceptable combinations that result in an extraction greater than 2.2%. These combinations are indicated in the red shaded area.

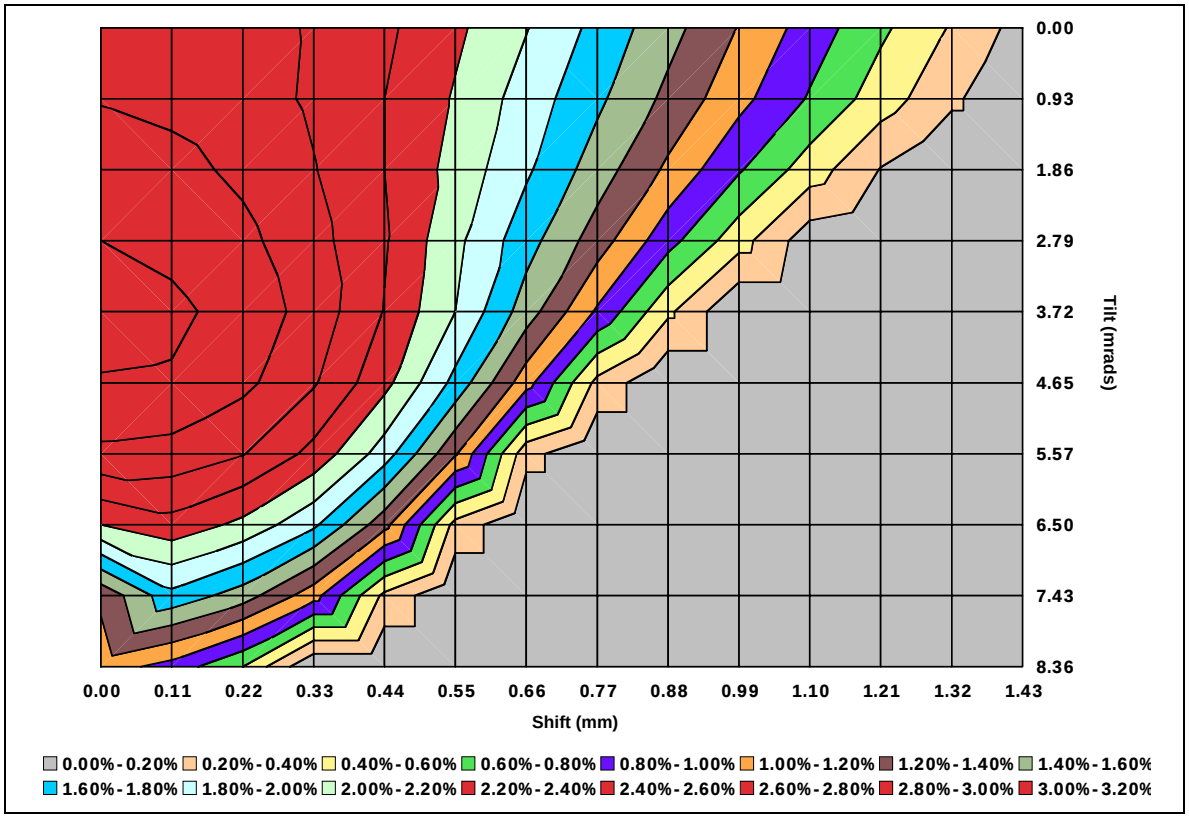

Figure 20. Extraction due to Electron Beam Shift with Tilt (Top View)

Additionally, Table 5 lists the extraction values for each combination simulated. Each simulation followed over 1000 passes of the optical beam through the undulator. This large number of passes was used to ensure saturation.

It can be seen in both Figure 20 and Table 5 that the largest shift allowable, with no tilt is approximately 0.55mm with a resultant extraction of 2.24%; this agrees with the

earlier simulations. These results will be used in the next section to determine the maximum allowable shift for each quadrupole magnet within the FEL beam path.

Shift		Tilt									
Dimensionless		0.0	1.0	2.0	3.0	4.0	5.0	6.0	7.0	8.0	9.0
	Actual	**0.00** mrads	**0.93** mrads	**1.86** mrads	**2.79** mrads	**3.72** mrads	**4.65** mrads	**5.57** mrads	**6.50** mrads	**7.43** mrads	**8.36** mrads
0	**0.00** mm	2.78%	2.79%	2.89%	3.00%	3.06%	2.99%	2.76%	2.20%	1.24%	1.10%
0.2	**0.11** mm	2.76%	2.75%	2.86%	2.95%	3.04%	2.98%	2.73%	2.33%	1.74%	0.92%
0.4	**0.22** mm	2.68%	2.69%	2.76%	2.85%	2.93%	2.85%	2.61%	2.15%	1.50%	0.60%
0.6	**0.33** mm	2.58%	2.57%	2.61%	2.67%	2.72%	2.62%	2.34%	1.84%	1.08%	0.00%
0.8	**0.44** mm	2.44%	2.40%	2.40%	2.42%	2.39%	2.26%	1.90%	1.27%	0.35%	0.00%
1	**0.55** mm	2.24%	2.18%	2.13%	2.05%	2.00%	1.74%	1.22%	0.33%	0.00%	0.00%
1.2	**0.66** mm	2.01%	1.91%	1.83%	1.68%	1.50%	1.08%	0.27%	0.00%	0.00%	0.00%
1.4	**0.77** mm	1.74%	1.64%	1.50%	1.30%	0.97%	0.34%	0.00%	0.00%	0.00%	0.00%
1.6	**0.88** mm	1.47%	1.35%	1.16%	0.87%	0.44%	0.00%	0.00%	0.00%	0.00%	0.00%
1.8	**0.99** mm	1.19%	1.06%	0.82%	0.48%	0.00%	0.00%	0.00%	0.00%	0.00%	0.00%
2	**1.10** mm	0.91%	0.78%	0.50%	0.08%	0.00%	0.00%	0.00%	0.00%	0.00%	0.00%
2.2	**1.21** mm	0.64%	0.50%	0.19%	0.00%	0.00%	0.00%	0.00%	0.00%	0.00%	0.00%
2.4	**1.32** mm	0.38%	0.24%	0.00%	0.00%	0.00%	0.00%	0.00%	0.00%	0.00%	0.00%
2.6	**1.43** mm	0.12%	0.00%	0.00%	0.00%	0.00%	0.00%	0.00%	0.00%	0.00%	0.00%

Table 5. Extraction due to Electron Beam Shift with Tilt Data

VI. FELSIM SIMULATIONS

A. FELSIM AND TRACE 3D OVERVIEW

FELSIM is a computer simulation tool developed in 2002 that incorporates many different modules from individual collaborators into one functional program. Collaborators that have contributed modules to this program include Advanced Energy Systems (AES), SAIC, Los Alamos National Laboratory (LANL), and Naval Postgraduate School (NPS).

This program is a systems code that utilizes an empirical approach to model different FEL designs. FELSIM can be run as a single program via AES's graphical user interface (GUI), or an individual module can be used for a more focused analysis. FELSIM is capable of optimizing an FEL to determine the system's efficiency, performance envelope and operational requirements. This program can also output approximate dimensions and weights of the FEL's components. Figure 21 is a typical FEL oscillator configuration used in FELSIM. [9]

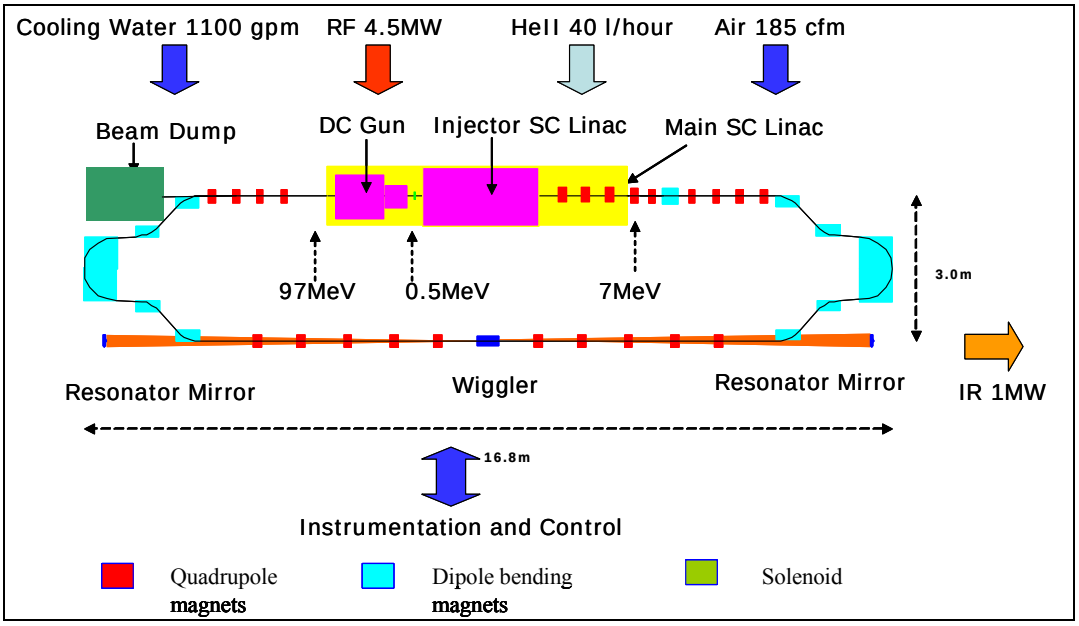

Figure 21. FELSIM 1MW Laser Layout. From [7]

Trace3D is one of the modules used in the FELSIM program. Trace3D was developed by LANL and is used in FELSIM to examine the evolution of the electron beam throughout the accelerator both before and after the wiggler (undulator). This is a beam-dynamics program that propagates the envelopes of bunched beams through a system. Trace3D will be extensively used in this study to analyze the resulting electron beam path due to quadrupole manipulations. [10]

In AES's September 2007 Monthly Report, funded by the Naval Surface Warfare Center, AES confirms the validity of using the Trace 3D module to simulate the displacement of a quadrupole magnet on the beam centroid. Therefore using Trace 3D to simulate linear quadrupole displacements is an acceptable method. [11]

B. FELSIM SET-UP FOR 1 MW DESIGN

The 1MW FEL design used for this study was generated by AES using FELSIM. The system was optimized based on beam dynamics for an electron beam on the reference trajectory. This design incorporates all components of an FEL previously discussed in Chapter 2 and displayed in Figure 21. However, for this study only a truncated section of the FEL design (from the end of the SLINAC to the beginning of the undulator) is used. This section is depicted in Figure 22.

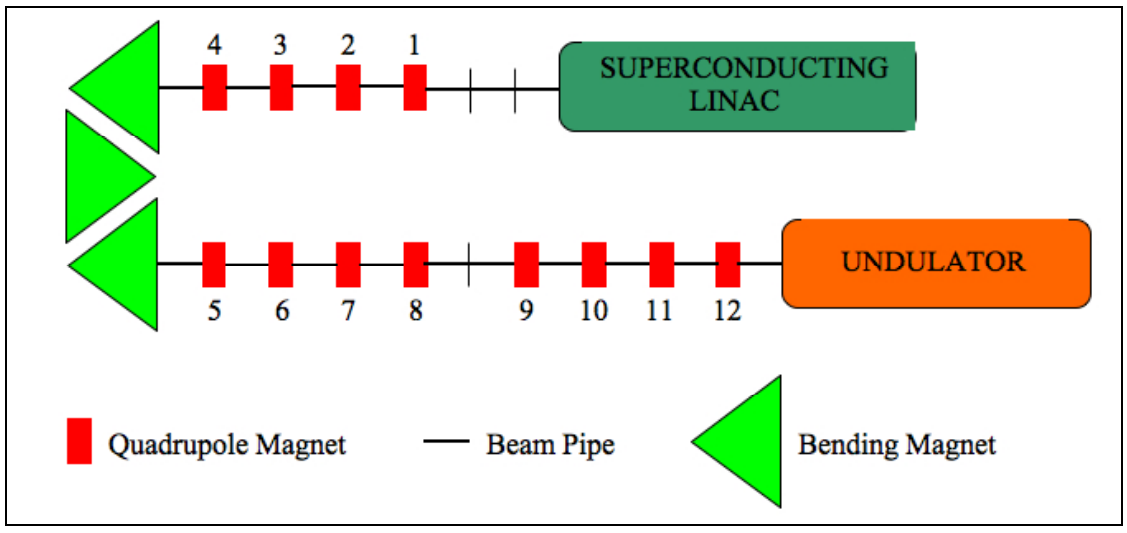

Figure 22. FELSIM Concatenated Section

This model contains a total of twelve quadrupole magnets, four before the turning magnets and eight between the bending magnet and the undulator. Each quadrupole is 150mm long; however, the magnetic gradient of each has been optimized using FELSIM based on an electron beam on a reference trajectory.

Table 6 indicates the length and placement of each component along the beam path starting at the exit of the SLINAC and ending at a distance of 10950mm at the beginning of the undulator. These values are important when calculating the matrix elements for the transport system, and identify the locations of the quadrupoles along the beam path.

Componet	**Z Placement** (mm)	**Componet**	**Z Placement** (mm)
SLINAC	0	Magnet 6	5991
drift	175	drift	6341
drift	411	Magnet 7	6491
drift	586	drift	6841
Magnet 1	736	Magnet 8	6991
drift	1086	drift	7844
Magnet 2	1236	drift	8697
drift	1586	Magnet 9	8847
Magnet 3	1736	drift	9197
drift	2086	Magnet 10	9347
Magnet 4	2236	drift	9697
drift	2411	Magnet 11	9847
Bending Magnet	2411	drift	10200
drift	5341	Magnet 12	10350
Magnet 5	5491	drift	10650
drift	5841	Oscillator	10950

Table 6. 1MW Component Start Position on Z-Axis

Table 7 shows the input data used in FELSIM for all simulations. The electron beam parameters are the same as those used in the 3D undulator simulations described in the previous chapter. Using the same data in both simulations will allow for a greater accuracy in quadrupole magnet disturbance tolerances.

RF frequency	748.5 MHz
Average current	458 mA
Initial Energy (out of Superconducting LINAC)	97.8 MeV
Initial Beam Radius	0.382 mm
Initial x emittance (unnormalized)	0.068 mm mrad
Initial y emittance (unnormalized)	0.056 mm mrad

Table 7. Initial Trace Input Data

1. Displacement of Magnet 1 through 4

Magnets 1 through 4 are positioned after the SLINAC and before the bending magnet. The gradients and following beam pipe are listed in Table 8. Magnets 1, 2, and 3 all have comparable gradients and Magnet 4 is much weaker, about a third the strength of the other three.

As discussed in Chapter II, there are two types of quadrupoles, "F" and "D", depending on their horizontal focusing. In this set of magnets, Magnets 1, 3, and 4 are all F type quadrupoles and therefore focus in the horizontal (x) direction. Magnet 2 is a D type and therefore focuses in the vertical (y) direction.

	Magnet 1	**Magnet 2**	**Magnet 3**	**Magnet 4**
Gradient (T/m)	-6.19	6.97	-6.16	-1.89
Beam Pipe Length After (mm)	350	350	350	175

Table 8. Magnet 1 through 4 Gradients and Beam Pipe

Figure 23 shows the results of quadrupole manipulation for the first four magnets (1-4) in the horizontal (x) direction. These graphs show the resulting horizontal electron beam shift and tilt (plotted on the vertical axis) at the beginning of the undulator as a function of the horizontal displacement of Magnets 1 through 4 (on the horizontal axis), where the magnet shift is in the positive horizontal direction.

Magnet 3 has the greatest impact on electron beam trajectory. Magnet 3 is limited to a horizontal shift of approximately 0.15mm that results in an electron beam shift of approximately 0.46mm and a tilt of 1.87mrads at the undulator assuming no other magnets are displaced. This corresponds to an extraction of about 2.40% from Figure 19. This greater response is due to the large gradient of Magnet 3 and the fact that it is an F

type quadrupole, therefore focusing in the direction of disturbance. Another factor is Magnet 3 placement in the beam line. This is the last horizontal focusing magnet before the bending magnet that has very weak horizontal focusing.

Magnet 4 has the least effect on electron beam shift. This magnet is limited to a horizontal displacement of 0.8mm, again assuming no other magnet is out of position. This corresponds to an electron beam shift of 0.41mm and a tilt of 1.89mrads at the undulator leading to an extraction of about 2.4%. This is mostly due to the lower gradient of the magnet.

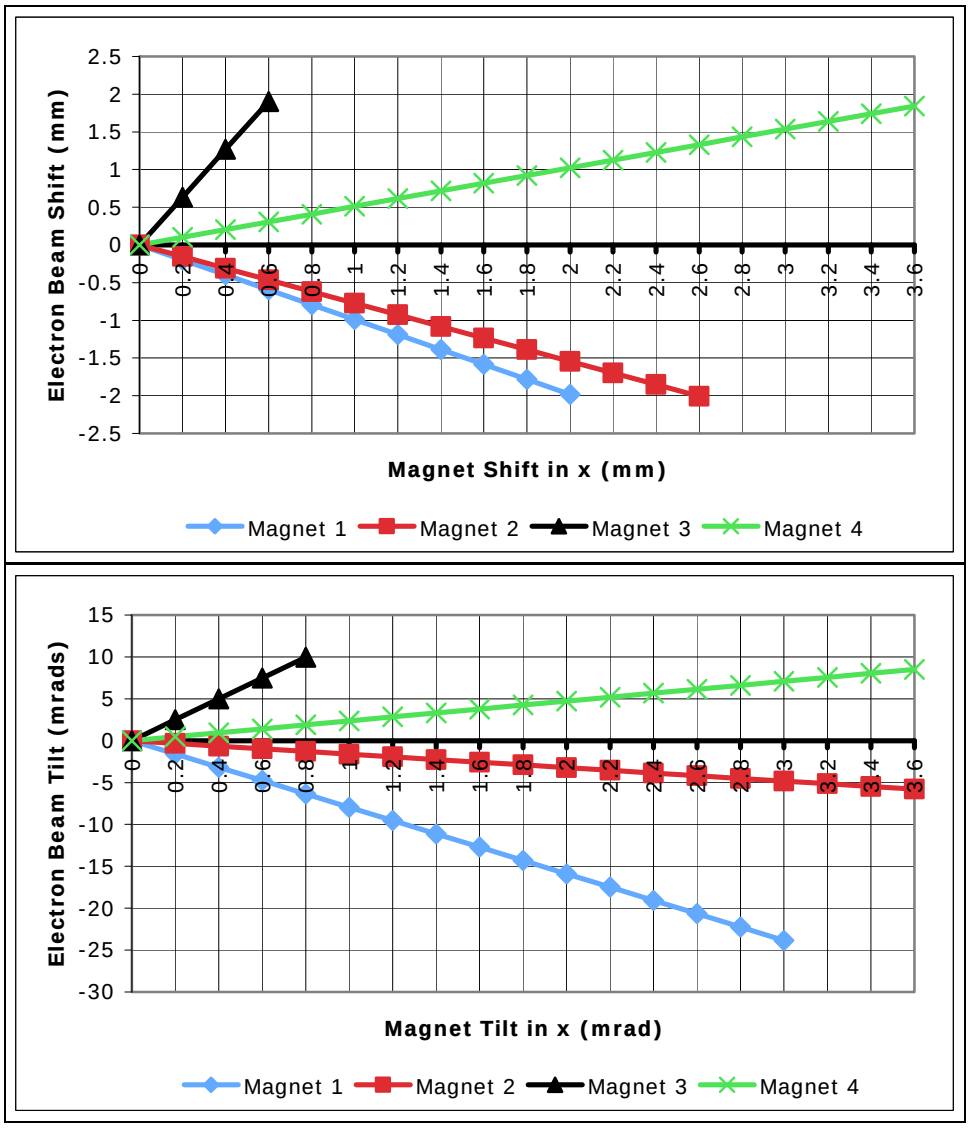

Figure 23. Beam Shift and Tilt due to Displacements in x

The results of quadrupole manipulation in the vertical (y) direction can be seen in Figure 24. This graph shows the resulting electron beam shift and tilt on the vertical axis resulting at the beginning of the undulator as a function of the vertical displacement, in millimeters on the horizontal axis, of Magnets 1 through 4 where the magnet shift is in the positive vertical direction.

It can be seen that the system has a greater sensitivity to a vertical shift of Magnet 2. Magnet 2 is limited to a vertical shift of approximately 0.03mm that results in an electron beam shift of 0.41mm and a tilt of 0.267mrads at the undulator. This corresponds to an extraction of approximately 2.44%. This greater response is due to the large gradient of Magnet 2 and the fact that it is a D type quadrupole, therefore focusing in the direction of disturbance.

Magnet 4 has the least effect on electron beam trajectory. This magnet is limited to a vertical displacement of 0.25mm, giving an extraction of approximately 2.24%. This is mostly due to the lower gradient and the fact that it is an F type quadrupole. It is important to note that the electron beam shift is a more limiting effect of these magnet displacements than is the beam tilt.

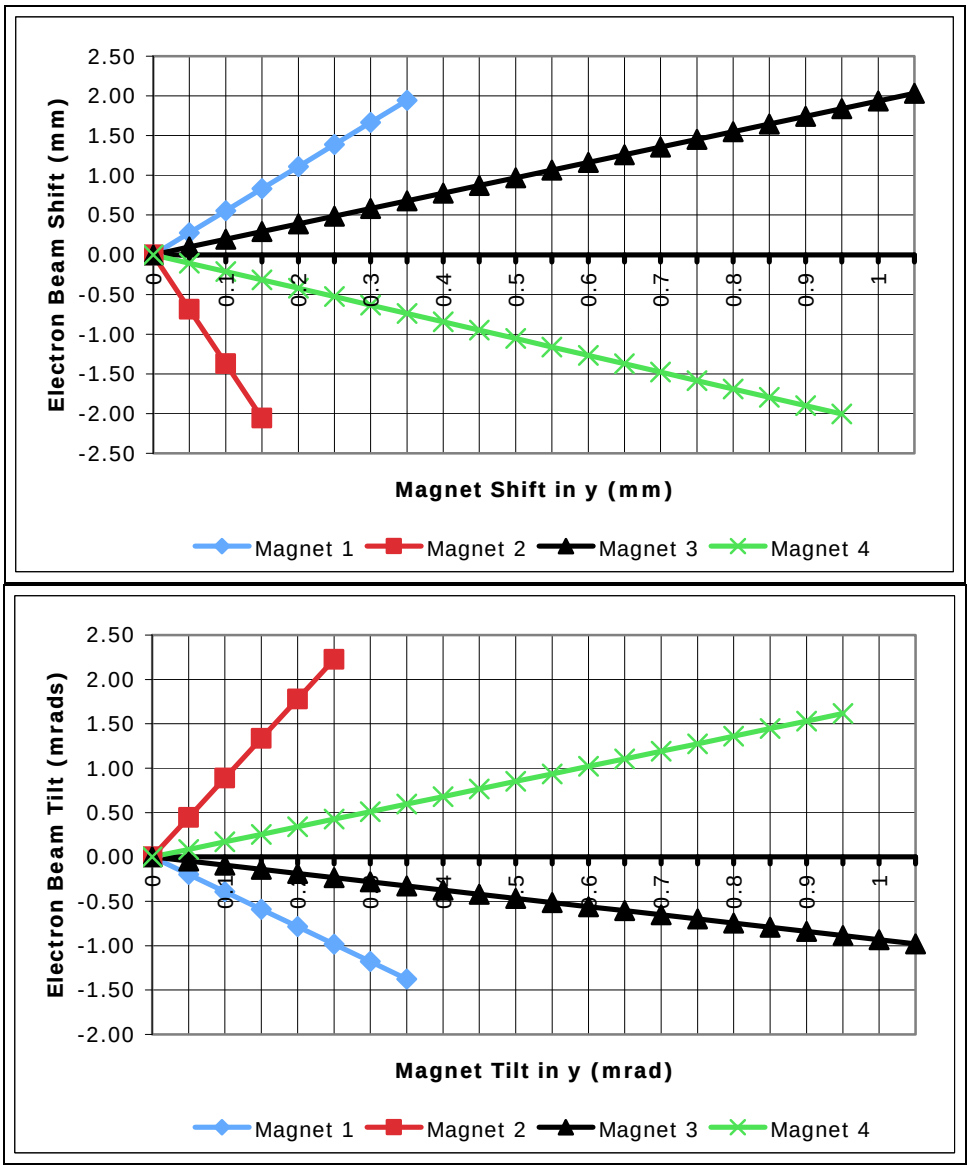

Figure 24. Beam Shift and Tilt due to Displacements in y

2. Displacement of Magnet 5 through 8

Magnets 5 through 8 are positioned directly after the bending magnet. The gradients and following beam pipe are listed in Table 9. Magnet 5 is much stronger than the other three magnets; in fact, its gradient is the most powerful in this concatenated section. Magnet 7 is about average compared to the next four magnets, while magnets 6 and 8 have very small gradients. While these values may not seem logical, they are the

result of the optimization process of the entire system done using FELSIM prior to these simulations. Magnets 8 would be considered an installed "tweaker" to a system. These quadrupoles would provide flexibility to the FEL and allow for future tuning.

In this set of magnets, Magnets 5 and 7 are F type quadrupoles and Magnets 6 and 8 are D type. Using the same analysis as previously discussed for Magnets 1 through 4 of this group, the system is most sensitive to disturbances of Magnet 5. Unlike the previous magnets, Magnet 5 is limited due to the large tilt created at the beginning of the undulator, not the horizontal shift, as can be seen in Figure 25. Magnet 5 is limited to approximately 0.15mm horizontal shift resulting in an electron beam shift of 0.2mm and a tilt of 5.94mrads at the undulator. This corresponds to an extraction of about 2.61%.

	Magnet 5	**Magnet 6**	**Magnet 7**	**Magnet 8**
Gradient (T/m)	-11.7	0.208	-4.37	.0004
Beam Pipe Length After (mm)	350	350	350	1706

Table 9. Magnet 5 through 8 Gradients and Beam Pipe

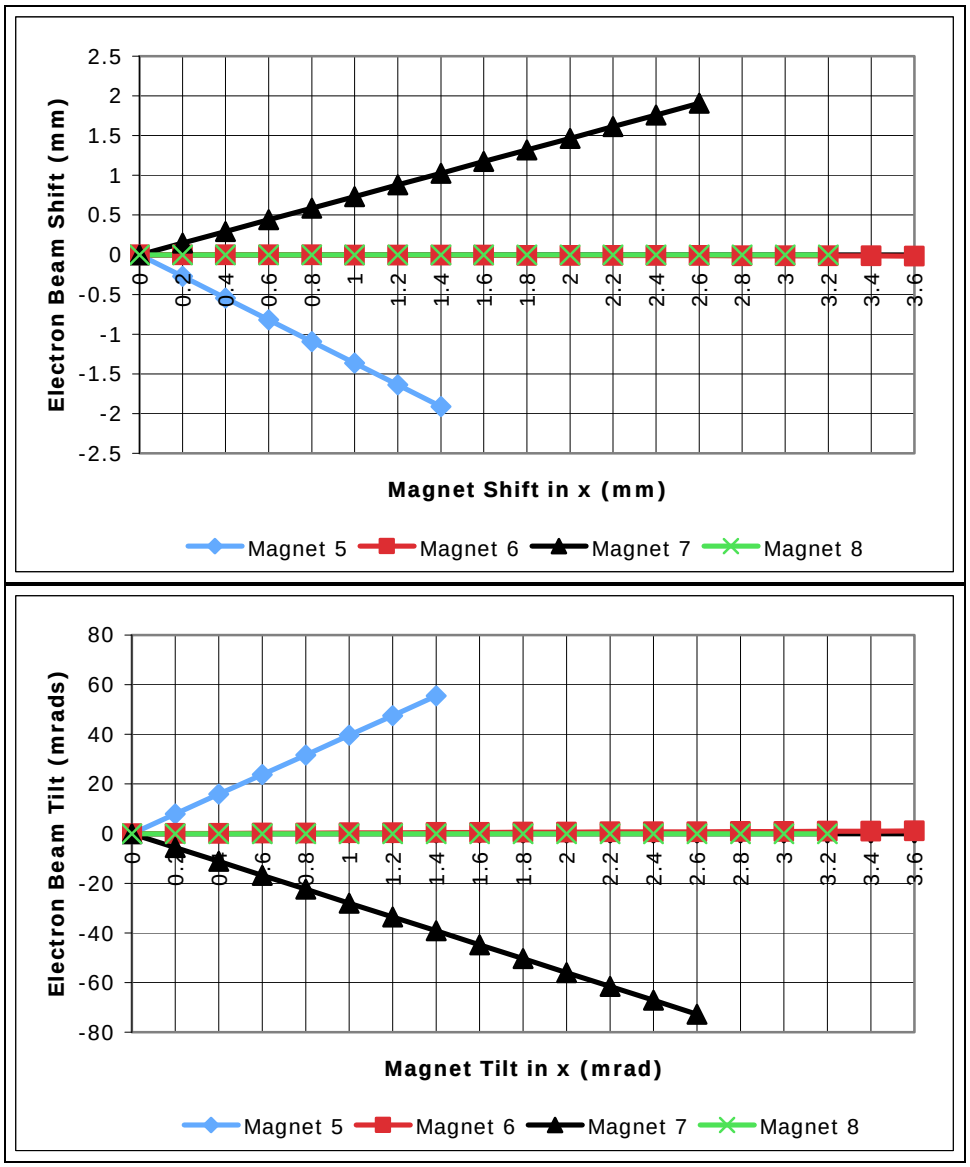

Figure 25. Beam Shift and Tilt due to Displacements in x

In the vertical direction, Magnet 5 is also the most sensitive. However, it is the resulting electron beam shift that is more limiting. Magnet 5 is limited to about 0.06mm of vertical displacement, resulting in an extraction of about 2.2%.

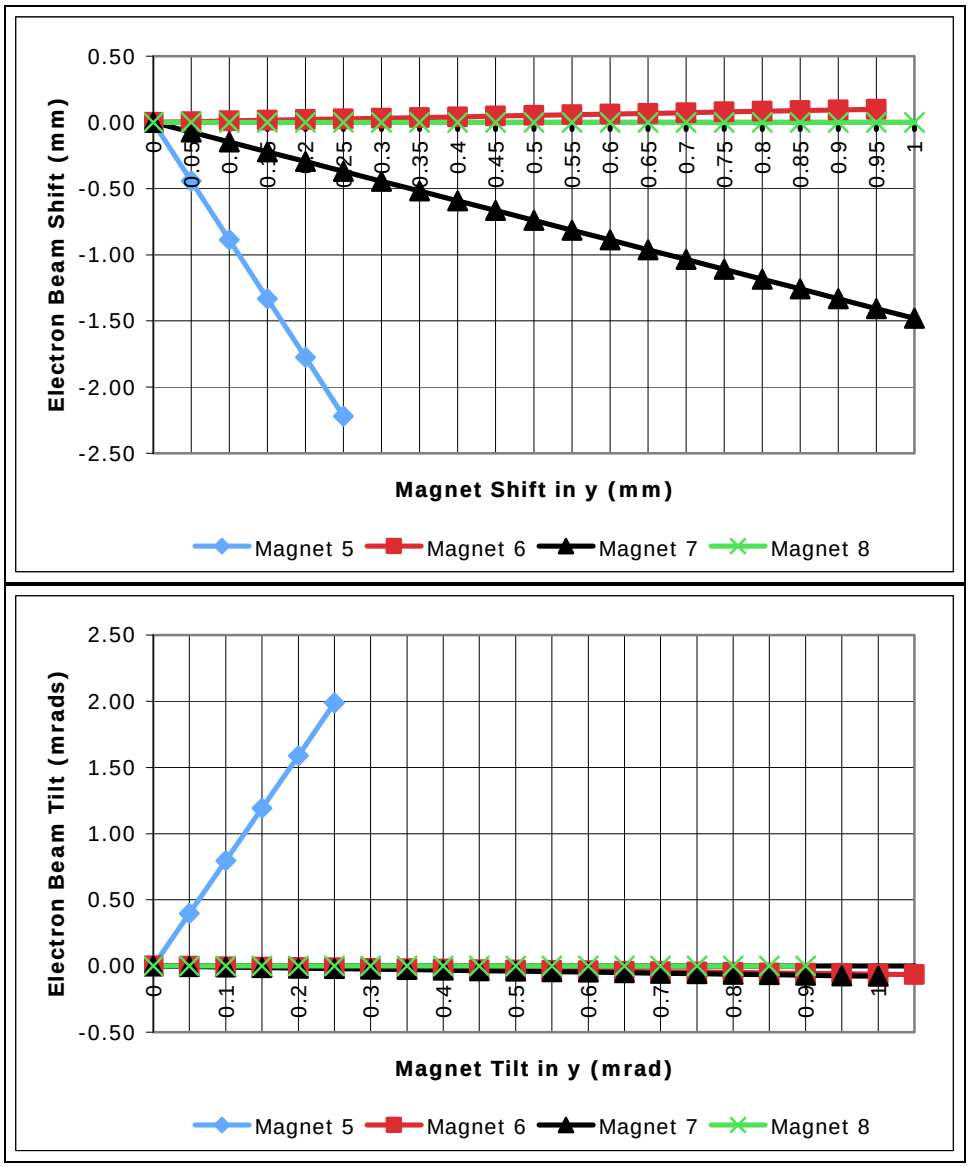

Figure 26. Beam Shift and Tilt due to Displacements in y

3. Displacement of Magnet 9 through 12

Magnets 9 through 12 are positioned just upstream of the undulator. The gradients and following beam pipes are listed in Table 10. Magnets 9, 10, and 11 all have comparable gradients and Magnet 12 is slightly larger. In this set of magnets, Magnets 10 and 12 are F type quadrupoles and Magnets 9 and 11 are D type.

	Magnet 9	Magnet 10	Magnet 11	Magnet 12
Gradient (T/m)	2.24	-2.63	3.85	-7.95
Beam Pipe Length After (mm)	350	350	350	300

Table 10. Magnet 9 through 12 Gradients and Beam Pipe

Figure 27 is the result of quadrupole manipulation in the horizontal (x) direction of these last four magnets. It can be seen that Magnet 12 has the greatest impact on electron beam trajectory. Magnet 12 is limited to a horizontal shift of approximately 0.4mm resulting in an extraction of about 2.40%. This greater response is due to the large gradient of Magnet 12 and the fact that it is an F type quadrupole.

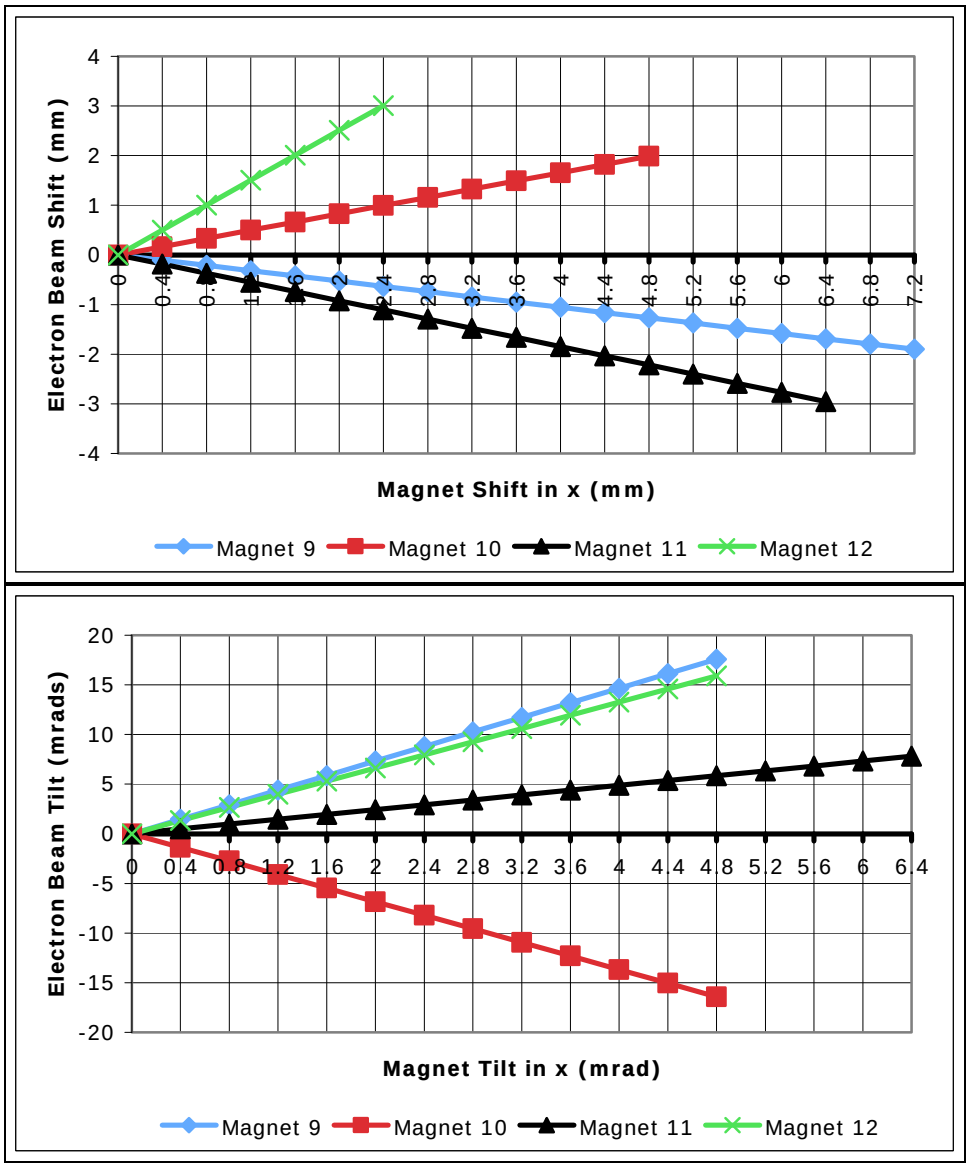

Figure 27. Beam Shift and Tilt due to Displacements in x

It can be seen on Figure 28 that the system has a greater sensitivity to a vertical shift of Magnet 11, a D type magnet. Magnet 11 is limited to a vertical shift of approximately 0.15mm that results in an electron beam shift of 0.41mm and a tilt of 0.75mrads at the undulator. This corresponds to an extraction of approximately 2.4%.

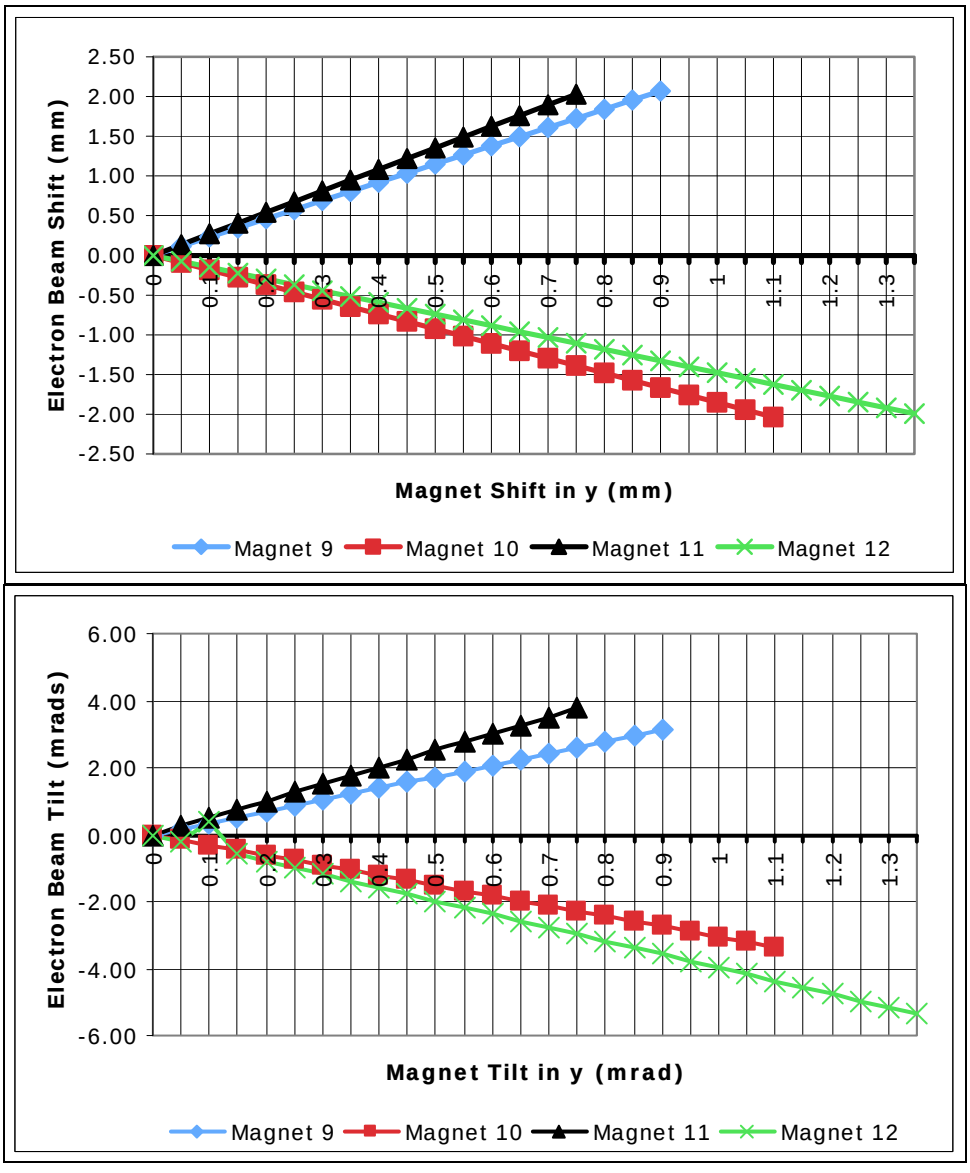

Figure 28. Beam Shift and Tilt due to Displacements in y

4. Electron Beam Evolution

While the FEL performance is only affected by the final shift of the electron beam, it is also important to analyze the intermediate steps through the transport system. Figure 29 and Figure 30 show the evolution of beam centroid offset from the end of the SLINAC to the beginning of the undulator within the concatenated section due to a disturbance of Magnet 1. On these two graphs the vertical axis represents the displacement, in millimeters, of the electron beam centroid from its reference trajectory and the horizontal axis represents the distance traveled along the beam line.

Figure 29 is a plot of the horizontal displacement of the electron beam throughout the concatenated section due to a 1mm horizontal shift of Magnet 1. This graph indicates what could be a significant problem. A typical beam pipe radius is approximately 15mm. This graph indicates that the electron beam will have a maximum displacement of 17.3mm. This beam shift is greater than the allowable clearance within the beam pipe and system components resulting in loss of beam and possible damage to the beam pipe and FEL system.

This maximum displacement occurs at Magnet 7. It can be seen that there is a large correction made to the electron beam trajectory at this point. This is due to the fact that Magnet 7 is an F type quadrupole and the separation between the beam and pole face is such that the electron beam experiences a large correctional force allowing the beam to move closer to centerline.

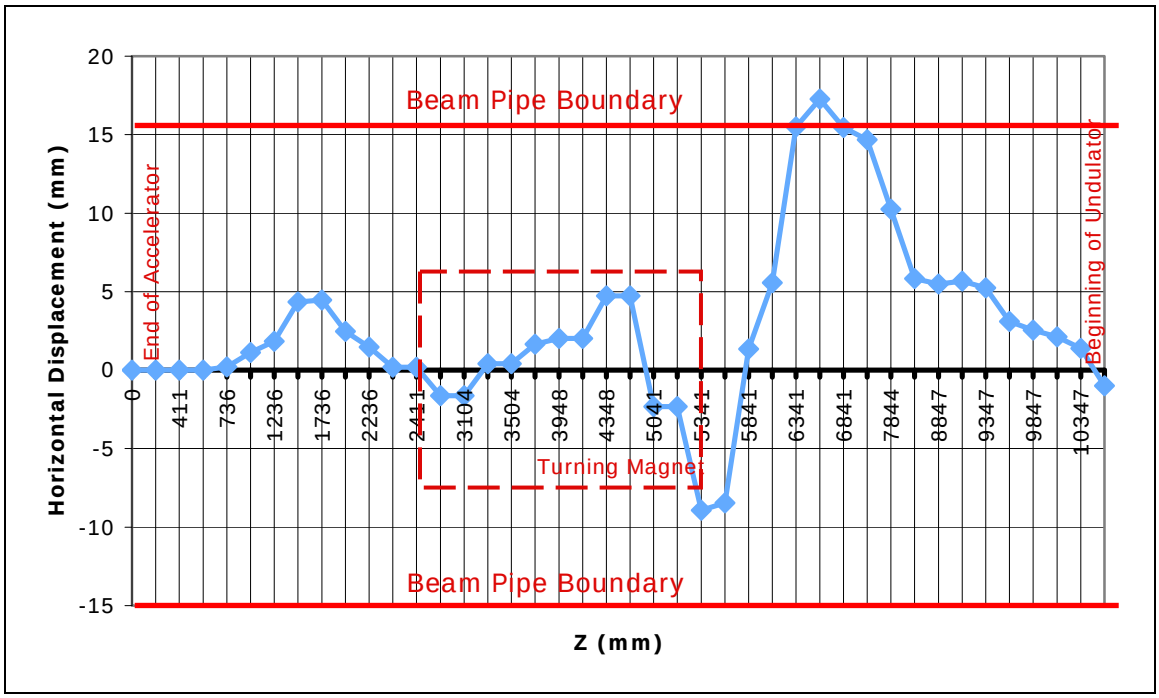

Figure 29. Beam Displacement for a 1mm Horizontal Displacement of Magnet 1

Figure 30 is a plot of the vertical displacement of the electron beam throughout the concatenated section due to a 0.2mm vertical shift of Magnet 1. This graph shows a less dramatic evolution (note the scale difference) with a maximum displacement of 4.47mm following Magnet 10.

A large correction is made to the electron beam's trajectory at z = 8847mm. This is the location of Magnet 9 as seen on Table 5. Because Magnet 9 is a D type quadrupole, therefore focusing in the vertical (y) direction and the distance between the beam and pole face is dramatically reduced; the electron beam experiences a large correctional force allowing the beam to move closer to centerline.

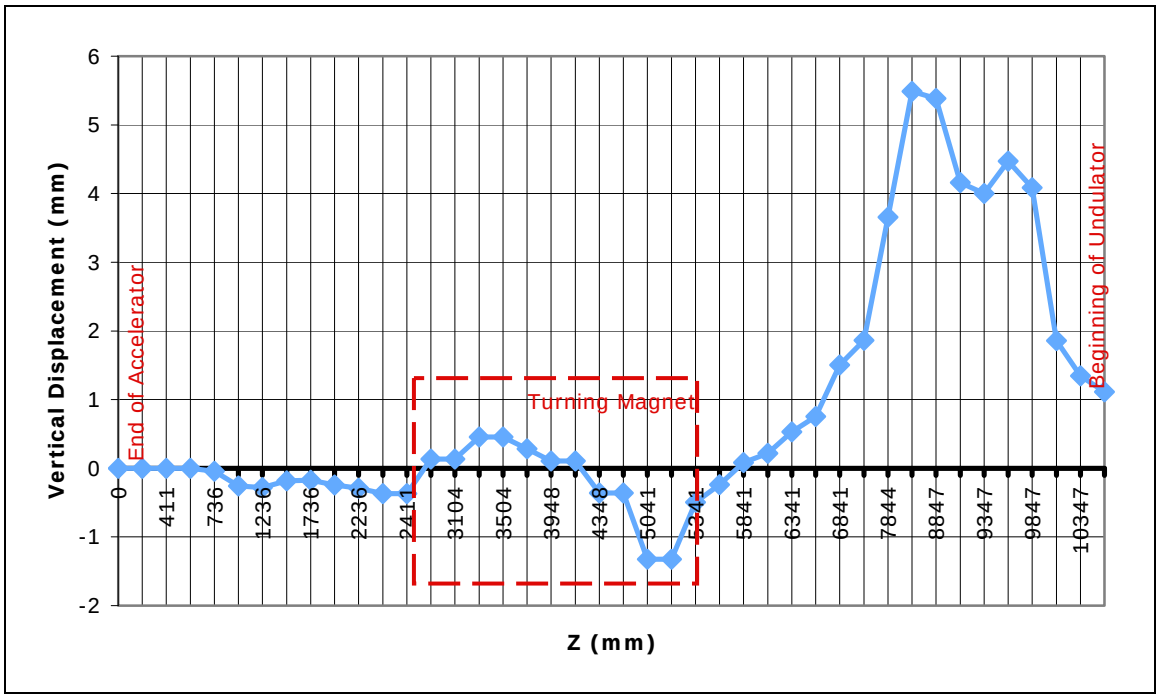

Figure 30. Beam Displacement for a 0.2mm Vertical Displacement of Magnet 1

C. SYSTEM DESIGN CRITERIA

To evaluate the system as a whole and establish system design tolerances, first it is important to establish criteria to set the limits of electron beam shift and tilt in order to maintain above 2.2% extraction. This equation will be that of an ellipse, within which all allowable combinations will fall. These equations will approximately fit the data found in Figure 5 and Table 20. The equations are

$$\left(\frac{\Delta x}{0.6\text{mm}}\right)^2+\left(\frac{\Delta x'}{6.45\text{mrad}}\right)^2\le 1 \text{ and} \tag{6.1}$$

$$\left(\frac{\Delta y}{0.6\text{mm}}\right)^2+\left(\frac{\Delta y'}{6.45\text{mrad}}\right)^2\le 1 \tag{6.2}$$

with Δx and Δy as the electron beam shifts and $\Delta x'$ and $\Delta y'$ as the tilts.

Table 11 is a list of all the slopes of the electron beam's response to magnets shifts found in Figures 23 to 28. Magnet displacements are labeled as δx, δy, whereas

the resulting responses of the electron beam at the undulator entrance are labeled as Δx, Δy, $\Delta x'$, and $\Delta y'$. It can be seen that the most sensitive magnets have the greatest slopes and therefore the greatest effect on electron beam trajectory.

		$\Delta x/\delta x$	$\Delta x'/\delta x \left(\text{mrad}/\text{mm}\right)$	$\Delta y/\delta y$	$\Delta y'/\delta y \left(\text{mrad}/\text{mm}\right)$
MAGNET	**1**	-0.99	-7.94	5.55	-3.93
	2	-0.77	-1.61	-13.71	8.90
	3	3.17	12.46	1.94	-0.93
	4	0.51	2.36	-2.11	1.70
	5	-1.37	39.62	-8.88	7.95
	6	0.00	0.30	0.11	-0.06
	7	0.73	-27.98	-1.48	-0.08
	8	0.00	0.00	0.00	0.00
	9	-0.26	3.66	2.30	3.45
	10	0.41	-3.42	-1.85	-3.05
	11	-0.46	1.22	2.71	5.02
	12	1.25	3.31	-1.48	-3.97

Table 11. Electron Beam Trajectory Responses (Δ) due to Magnet Displacement (δ)

Using these slopes, an overall system tolerance can be established to first order by assuming all twelve magnets have the same range of motion but are otherwise uncorrelated. The average of the squared electron beam shift and tilt in the vertical and horizontal direction can be found by summing the square of the slopes; these equations are

$$\left\langle \Delta x^2 \right\rangle = \left\langle \delta x^2 \right\rangle \left(\left(\Delta x/\delta x_1 \right)^2 + \left(\Delta x/\delta x_2 \right)^2 + \left(\Delta x/\delta x_3 \right)^2 + \ldots \left(\Delta x/\delta x_{12} \right)^2 \right), \tag{6.3}$$

$$\left\langle \Delta y^2 \right\rangle = \left\langle \delta y^2 \right\rangle \left(\left(\Delta x/\delta y_1 \right)^2 + \left(\Delta x/\delta y_2 \right)^2 + \left(\Delta x/\delta y_3 \right)^2 + \ldots \left(\Delta x/\delta y_{12} \right)^2 \right), \tag{6.4}$$

$$\left\langle \Delta x'^2 \right\rangle = \left\langle \delta x^2 \right\rangle \left(\left(\Delta x/\delta x'_1 \right)^2 + \left(\Delta x/\delta x'_2 \right)^2 + \left(\Delta x/\delta x'_3 \right)^2 + \ldots \left(\Delta x/\delta x'_{12} \right)^2 \right), \text{ and} \tag{6.5}$$

$$\left\langle \Delta y'^2 \right\rangle = \left\langle \delta y^2 \right\rangle \left(\left(\Delta y / \delta y'_1 \right)^2 + \left(\Delta x / \delta y'_2 \right)^2 + \left(\Delta x / \delta y'_3 \right)^2 + \ldots \left(\Delta x / \delta y'_{12} \right)^2 \right) \qquad (6.6)$$

Where δx_j is the displacement of the j_{th} magnet $\left(j = 1 \rightarrow 12 \right)$.

Using the limits found in the previous chapter of Δx and $\Delta y = 0.6\text{mm}$ shift and $\Delta x'$ and $\Delta y' = 6.5\text{mrads}$ tilt, equations (6.3) to (6.5) can be combined with equations (6.1) and (6.2) to give the average allowable squared magnet displacements as

$$\left\langle \Delta x^2 \right\rangle = \left\langle \delta x^2 \right\rangle \cdot 16.3\text{mm}^2, \qquad \left\langle \Delta x'^2 \right\rangle = \left\langle \delta x'^2 \right\rangle \cdot 2620 \frac{\text{mrad}^2}{\text{mm}^2},$$

$$\left\langle \Delta y^2 \right\rangle = \left\langle \delta y^2 \right\rangle \cdot 326\text{mm}^2, \text{ and} \qquad \left\langle \Delta y'^2 \right\rangle = \left\langle \delta y'^2 \right\rangle \cdot 224 \frac{\text{mrad}^2}{\text{mm}^2}.$$

Using (6.1) and 6.2), the overall vertical and horizontal magnet shift of the entire system as a whole is calculated using (6.1) and (6.2) as

$$\delta x_{\text{MAX}} \leq \frac{1}{\sqrt{\frac{(16.3)}{\left\langle (0.6\text{mm})^2 \right\rangle} + \frac{(2620)}{\left\langle (6.5\text{mrad})^2 \right\rangle}}} \longrightarrow \delta x_{\text{MAX}} \leq 0.097\text{mm} \text{ and}$$

$$\delta y_{\text{MAX}} \leq \frac{1}{\sqrt{\frac{(326)}{\left\langle (0.6\text{mm})^2 \right\rangle} + \frac{(224)}{\left\langle (6.5\text{mrad})^2 \right\rangle}}} \longrightarrow \delta y_{\text{MAX}} \leq 0.033\text{mm}.$$

Therefore, the maximum horizontal and vertical magnet system shift tolerances are 0.097mm and 0.033mm, respectively. It is important to note that this approximation will give tolerances that would allow approximately a 50% probability of meeting the 2.2% extraction limit. To improve this probability the tolerances must be reduced. To improve on this first-order approximation, a Monte Carlo-type analysis is required to examine nonlinear effects. This analysis will allow changes to transverse electron beam shape as well as position. Additionally, this study will more precisely map out the region of in-tolerance operation approximated by equations (6.1) and (6.2). Other studies required are the exploration of simultaneous and coupled oscillations in the x and y planes.

THIS PAGE INTENTIONALLY LEFT BLANK

VI. CONCLUSION

This analysis has provided the beginning ground work for the study of quadrupole magnet misalignments in an FEL weapon system in a shipboard environment. Using the 3D FEL Oscillator Simulator developed at NPS, limits were established to ensure the FEL would operate at 1MW or greater. These simulations revealed that for this FEL system a minimum extraction of 2.2% was required to achieve this power requirement. Following a multitude of simulations, operating limits on the electron beam shift and tilt were found. The results allow tolerances to be set prior to the study of quadrupole magnet misalignments. It was found that the maximum shift allowed, with no tilt is 0.6mm and a maximum tilt allowed, with no shift is 6.5mrads. However, because a typical magnet misalignment on a ship could cause both shift and tilt, the tolerance for both shift and tilt is evaluated in the combination.

Using Trace3D, a module of FELSIM, each of the twelve quadrupole magnets was individually shifted. Maximum allowable shifts varied in both the horizontal and vertical directions due to placement and field strength. The allowed shifts were on the order of tenths of millimeters with the most limiting in this system at 0.06mm. Using the results found in FELSIM, an overall system tolerance (if all magnets vibrated with the same amplitude) was found to be 0.097mm horizontal shift and 0.033mm vertical shift.

These maximum quadrupole shifts for system vibrations are smaller than the typical amplitude of ship vibrations on a Naval vessel. Therefore, both vibration dampening and active alignment need to be used to minimize these disturbances to less than the tolerances found. This can and has been achieved in other military and scientific endeavors such as the Airforce's Airborne Laser (ABL) program. [12]

Future work should continue this study by utilizing a Monte Carlo-type analysis to examine nonlinear effects of quadrupole shifts. Another related topic requiring research is the effect of quadrupole magnet tilts due to flexing and bending of the ship.

THIS PAGE INTENTIONALLY LEFT BLANK

LIST OF REFERENCES

[1] Jefferson Labs. "Thomas Jefferson National Accelerator Facility," July 2007. [www.jlab.org/FEL/felspecs.html].

[2] CMS Alphatech. "Magnets," August 2007. [www.cmsalphatech.com/magnets.htm].

[3] Neil Thomson. "Introduction to Free-Electron Lasers," ASTeC. July 2007.

[4] B.Williams. "Higher-order modes in free electron lasers," Master's thesis, Naval Postgraduate School, 2005.

[5] John David Jackson. *Classical Electrodynamics*, 3rd Edition. John Wiley & Sons Inc. 1999. 220, 586.

[6] W. B.Colson. Naval Postgraduate School,
a. PH4858 Class Lecture. NPS. Fall 2006.
b. C. Pellegrini and A. Renieri. *Classical Free Electron Laser Theory*, Chapter 5 in "Free Electron Laser Handbook," Elsevier Science Publishing Co. Inc. December 1990.

[7] David C. Carey. *The Optics of Charged Particle Beams*, Harwood Academic Publishers. 1987. 261-271.

[8] Martin Reiser. Theory and Design of Charged Particle Beams, John Wiley & Sons Inc. 1994. 111-116.

[9] Advanced Energy Systems. "FELSIM Overview: Accelerator Beam Dynamics using Trace 3D," January 2007.

[10] K.R. Crrandall and D.P. Rusthoi. "Trace 3-D Documentation 3rd ed," Los Alamos National Laboratory. 1997.

[11] Alan Todd. "Technical Services to Design, Develop, Demonstrate, Test and Deliver Engineering Test Units in Support of the Navy Free Electron Laser Project," Advance Energy Systems. September 2007.

[12] C. Allen. "Integrating the FEL on an All-Electric Ship," Master's thesis, Naval Postgraduate School, 2007.

THIS PAGE INTENTIONALLY LEFT BLANK

INITIAL DISTRIBUTION LIST

1. Defense Technical Information Center
   Ft. Belvoir, Virginia

2. Dudley Knox Library
   Naval Postgraduate School
   Monterey, California

3. William B. Colson
   Naval Postgraduate School
   Monterey, California

4. John W. Lewellen
   Naval Postgraduate School
   Monterey, California